

OUTP-93-18P

DFTT 9/93

hep-th/9308322

August 1993

**ANOMALOUS EVOLUTION OF THE GOTTFRIED SUM**Richard D. Ball<sup>\*</sup>*Theoretical Physics, University of Oxford  
1 Keble Road, Oxford OX1 3NP, U.K.*

and

Stefano Forte<sup>\*</sup>*I.N.F.N., Sezione di Torino  
via P. Giuria 1, I-10125 Torino, Italy***Abstract**

We discuss nonperturbative QCD evolution of nonsinglet nucleon structure functions, with particular application to the Gottfried sum. We show that the coupling of the quark partons to bound state mesons leads to nonperturbative contributions to the Altarelli–Parisi equations which, due to the axial anomaly, result in a strong scale dependence of nonsinglet structure functions for values of  $Q^2$  around the nucleon mass scale. We compute specifically the evolution of the first moment of the quark distribution, and find that it is

---

<sup>\*</sup> Address from October 1993 (RDB) and December 1993 (SF): Theory Division, CERN, CH–1211 Genève 23, Switzerland.

sufficient to explain recent experimental data which indicate a violation of the Gottfried sum rule.

Submitted to: *Nuclear Physics B*

## 1. Violation of the Gottfried Sum Rule

In the wake of the furore over the EMC measurement [1] of quark polarized structure functions, experimental results from the NMC[2] for the Gottfried sum again appear to be in contradiction with theoretical expectations. More specifically, the NMC measure the ratio of the cross-sections for unpolarized deep-inelastic scattering from deuterium and hydrogen targets. The ratio of structure functions  $F_2^d(x, Q^2)/F_2^p(x, Q^2)$  is extracted in the range  $0.004 \leq x \leq 0.8$  at  $Q^2 = 4 \text{ GeV}^2$ . Extrapolating to small  $x$  using Regge behaviour, and assuming further that the neutron structure function is just  $F_2^n = 2F_2^d - F_2^p$  allows a determination of the Gottfried sum, defined as

$$S_G \equiv \int_0^1 \frac{dx}{x} [F_2^p(x) - F_2^n(x)], \quad (1.1)$$

with the result

$$S_G = 0.24 \pm 0.016 \quad \text{at} \quad Q^2 = 4\text{GeV}^2. \quad (1.2)$$

This result (unlike previous less precise experimental determinations which had a consistent central value but larger errors) is in striking contradiction with the Gottfried sum rule, which would have  $S_G = \frac{1}{3}$  [3].

Both of the assumptions used by the NMC to arrive at the result (1.2) may be questioned: on the one hand, if Regge behaviour is assumed to set in only at very small  $x$  ( $\sim 10^{-3}$  or less) it is not difficult to increase  $S_G$  [4], while on the other if nuclear shadowing is taken into account the neutron structure function is certainly larger than the difference between deuterium and proton structure functions, thus leading to a yet smaller value of  $S_G$ , perhaps[5] around or even below  $S_G \sim 0.2$ . The settling of these issues rests ultimately with experiment, and in particular with the availability of better data in the small- $x$  region. However, if we accept that the result (1.2) is correct, perhaps with slightly underestimated error, we must conclude that the Gottfried sum rule does not hold at the scale of the NMC measurement.

Let us therefore review how this sum rule is derived. In the parton model,  $F_2(x)$  is related to the sum of parton densities, weighted by the electric charges squared (see e.g.[6]):

$$F_2(x) = x \sum_i e_i^2 (q_i(x) + \bar{q}_i(x)), \quad (1.3)$$

where  $q_i(x)$  ( $\bar{q}_i(x)$ ) is the quark (antiquark) density of flavor  $i$ . This identification is exact (by definition) to all orders in the QCD parton model. Although the first moments of  $q_i(x)$

and  $\bar{q}_i(x)$  diverge because of their small- $x$  behaviour, this divergence is expected to cancel in nonsinglet combinations of quark distributions (such as in the Gottfried sum), on the basis the small- $x$  behaviour of  $q_i(x)$  expected from Regge theory[7].

It follows that the Gottfried sum measures the difference between the sums of the square charges of partons (quarks *plus* antiquarks) in proton and neutron. Assuming exact isospin symmetry

$$S_G = \int_0^1 dx (e_u^2 - e_d^2)(q_u(x) - q_d(x) + \bar{q}_u(x) - \bar{q}_d(x)) = \frac{1}{3}(q_1 + \bar{q}_1), \quad (1.4)$$

where  $q_1$  and  $\bar{q}_1$  are the first moments of the nonsinglet quark distributions

$$q(x) \equiv q_u(x) - q_d(x), \quad \bar{q}(x) \equiv \bar{q}_u(x) - \bar{q}_d(x). \quad (1.5)$$

On the other hand, one may derive an exact sum rule (the Adler sum rule) for the charge-conjugation odd combination of first moments which counts quarks *minus* antiquarks. By charge conservation this is fixed:

$$S_A \equiv q_1 - \bar{q}_1 = 1. \quad (1.6)$$

Only valence quarks contribute to the Adler sum rule, since (by definition)  $q_1^{\text{sea}} = \bar{q}_1^{\text{sea}}$ , while the Gottfried sum receives contributions from both valence and sea quarks. However if we assume further that the quark–antiquark sea is isotopically neutral, then  $\bar{q}_1 = \bar{q}_1^{\text{sea}} = 0$ , and we find (using (1.6) in (1.4)) the naive result  $S_G = \frac{1}{3}$  alluded to above.

The NMC result (1.2) thus suggests that the light flavor content of the nucleon is very different from the standard folklore[8] of an asymmetric valence quark content, plus sea quark, antiquark and gluon distributions which respect all possible symmetries. In particular, a detailed analysis[9] indicates that isospin violations (such that the total number of sea quark–antiquark pairs in the proton and in the neutron are not exactly the same) cannot by themselves account for the discrepancy; the value (1.2) requires a large violation of the SU(2) symmetry of the quark–antiquark sea, such that the number of up quark–antiquark pairs in each nucleon must be different from the number of down pairs. More precisely, the NMC data require[9] the isospin violation to be  $\lesssim 5\%$ , and the sea asymmetry to be opposite in sign to the valence asymmetry, and about 30% of its magnitude. Thus (recalling eqn.(1.6))  $q_1^{\text{sea}} + \bar{q}_1^{\text{sea}} \sim -0.3$ , and not zero as naively assumed.

This conclusion is not only unsettling from the phenomenological point of view, given that the naive assumption of a symmetric sea is embodied in all phenomenological parameterizations of parton distributions which are used in analyzing deep-inelastic scattering data<sup>1</sup>, but is also puzzling from the theoretical viewpoint. Indeed, one might expect the quark-antiquark sea probed in deep-inelastic scattering to be mostly produced through QCD evolution. But the scale dependence of  $S_G$  as computed perturbatively at two loops in QCD[11] is negligibly weak<sup>2</sup>, leading to a variation of  $S_G$  by less than 1% in the perturbative region. Furthermore, the same computation[11] shows explicitly that the naive explanation[12] of the sea asymmetry as a consequence of the Pauli principle (according to which the emission of sea up pairs in the proton should be reduced due to the up excess in the valence component [13]) is incorrect: due to subtle interference effects the Pauli antisymmetrization actually leads to a slight perturbative enhancement of the sea flavor asymmetry with the same sign as the valence asymmetry.

It has been suggested [12,14,15] that the effect may instead be related to the presence of a pion cloud in the nucleon wave function. Indeed, if one assumes that some portion of the sea is produced through transitions where a pion is radiated by a nucleon, then a proton would seem to favor the transition where a  $\pi^+$  is created, namely  $p \rightarrow n + \pi^+$ , over that where a  $\pi^-$  is created, namely  $p \rightarrow \Delta^{++} + \pi^-$  (and conversely for a neutron), because of the nucleon- $\Delta$  mass difference. This, spelling out the quark content, is seen to favor the production of  $d\bar{d}$  pairs over  $u\bar{u}$  pairs, thus producing a flavor asymmetry with the right sign. The observed effect may also be accommodated rather easily in most of the various effective models of the nucleon; examples are the Skyrme model[9,16], chiral soliton models [17], and various bag models[9,18].

The problem with this kind of explanation is not only that it is difficult to make quantitative and model-independent predictions, but that the connection between the models (which are presumably only valid at some unknown but low energy scale) and the parton distributions measured by the NMC is not at all clear. Furthermore, even accepting that pion effects are somehow responsible for the observed asymmetry, it is not enough[9] to assume that the  $\pi^+$  and  $\pi^-$  clouds in a nucleon are unequal, since each pion gives a vanishing contribution to the flavor asymmetry of the quark sea. Rather, one has to make a separate dynamical assumption on the pion production mechanism, in order to obtain

---

<sup>1</sup> Recently new parameterizations have appeared, which incorporate the NMC asymmetry[10].

<sup>2</sup> Though not zero, as seems to be sometimes believed (see for example ref.[8]).

an anticorrelation between valence and sea asymmetries. Such a mechanism has been presented in ref.[19], where it is shown that if (part of) the sea is produced by dissociation of a quark into a quark plus a pion, then the breaking of the axial U(1) symmetry in the pseudoscalar spectrum favors flavor-changing transitions over flavor-preserving ones. A calculation [19] based on the chiral quark model of ref.[20] seems to support this idea.

It is interesting to compare this situation with a similar instance of the failure of naive expectations, namely that of the Ellis–Jaffe sum as measured by the EMC[1] (for reviews see ref.[21]). In that case too the first moment of a nucleon structure function (the polarized proton structure function  $g_1^p$ ) is found to be considerably smaller than the parton model expectation, implying that the quark contribution to the “proton spin” (more precisely, its isosinglet axial charge) is consistent with zero. There, however, perturbative QCD suggests a partial explanation of the observed effect: due to the axial anomaly, the isosinglet axial charge evolves, despite being classically conserved. This evolution may be interpreted in the parton model by writing the charge as a sum of a polarized quark contribution (which does not evolve) and an anomalous gluon contribution (which does). Whereas the perturbative evolution (which, again, only occurs at two loops) is too weak to explain why the gluon contribution is so large, the observed discrepancy could be explained by a nonperturbative dynamical mechanism which generates a gluon contribution of the appropriate sign and magnitude. Such a mechanism would incorporate the same infrared non-perturbative physics that resolves the U(1) problem by giving a mass to the flavor singlet pseudoscalar meson (the  $\eta_0$ ) [22]. It could take the form of infrared vacuum effects (as modelled for example by instantons) [23] which reduce the starting value of the charge, or a non-perturbatively induced scale dependence of the isosinglet axial charge [24].

Here we will show that the anomaly also affects the non-perturbative evolution of the Gottfried sum, albeit in a rather more subtle way. We compute the non-perturbative scale dependence of nonsinglet quark structure functions by including bound state emission, thereby generalizing the usual Altarelli–Parisi evolution equations. We find that when the axial anomaly is taken into account through the generation of a mass for the  $\eta_0$  (as suggested in ref.[19]), then a flavor asymmetry in the quark sea is generated dynamically and the Gottfried sum acquires a rather strong scale dependence over intermediate scales. At very large and very small scales this dependence flattens out, so that the two loop perturbative evolution eventually takes over at large  $Q^2$ , whereas a constant “quark model” value is attained in the infrared region. We find that if this is identified with the

naive expectation  $S_G = 1/3$ , then the experimental value of  $S_G$ , eqn.(1.2), can be easily reproduced.

The paper is organized as follows: in section 2 we review the general theory of the  $Q^2$  dependence of the nonsinglet structure function  $F_2$ , both from the point of view of the operator-product expansion, and the QCD parton model; in section 3 we generalize the latter approach to include non-perturbative coupling to mesonic bound states, we describe the determination of the nonperturbative contribution to the anomalous dimensions, and we discuss how this can lead to flavor symmetry breaking effects due to the U(1) anomaly; in section 4 we compute the non-perturbative contribution to the appropriate splitting functions by explicit determination of the relevant cross-sections; in section 5 we determine the  $Q^2$  dependence of the first moment of the quark distribution, hence of the Gottfried sum, and compare our results with the NMC data; and finally in section 6 we summarize our results and discuss how this approach may be developed into a more general technique for the computation of nonperturbative contributions to structure function evolution.

## 2. Evolution of Nonsinglet Quark Distributions

Because the structure functions  $F_2(x)$  are proportional (1.3) to the quark distributions  $q_i(x)$ , the problem of the determination of their  $Q^2$  dependence reduces to the computation of the QCD evolution of the latter. Since we are only interested in the difference  $F_2^p(x) - F_2^n(x)$ , we need only discuss the evolution of the nonsinglet distributions  $q(x)$  defined in (1.5), although most of what follows would apply equally to other nonsinglet distributions.

We begin with a discussion of the evolution as dictated by the operator product expansion[11]. This is not straightforward, because the (electromagnetic) structure functions  $F_2$  are even under charge conjugation, as eqn.(1.3) demonstrates explicitly. It follows that at leading twist only the even moments of  $F_2$  can be expressed as the matrix element of a local operator, since the leading-twist contribution to the  $N$ -th moment has spin  $N$  hence charge conjugation  $\mathcal{C} = (-)^N$ . As shown in ref.[11], however, this does not imply that it is impossible to give a meaning to odd moments of  $F_2^p$  or their evolution, as is sometimes claimed[25].

Indeed, consider the combinations

$$q^\pm(x; t) = q(x; t) \pm \bar{q}(x; t), \quad (2.1)$$

where we have indicated explicitly the dependence on the scale  $t \equiv \ln Q^2/\mu^2$ . Since  $q^\pm$  are eigenstates of charge conjugation, they evolve independently. Even moments of  $q^+$  and odd moments  $q^-$  have the scale dependence

$$\begin{aligned} q_N^+(t) &= \Delta_N(t, t_0) q_N^+(t_0), & N \text{ even}, \\ q_N^-(t) &= \Delta_N(t, t_0) q_N^-(t_0), & N \text{ odd}, \end{aligned} \quad (2.2)$$

where  $q_N^\pm(t) \equiv \int_0^1 dx x^{N-1} q^\pm(x; t)$  is the  $N$ -th moment of  $q^\pm(x; t)$ ,  $t_0 \equiv \ln Q_0^2/\mu^2$ , and the scaling factor  $\Delta_N(t, t_0)$  is given in terms of the anomalous dimensions  $\gamma_N(t)$  of the twist-2, spin- $N$  nonsinglet local operators by

$$\ln \Delta_N(t, t_0) = \int_{t_0}^t \gamma_N(t') dt'. \quad (2.3)$$

If we let

$$\gamma_N = \gamma_N^{qq} + (-)^N \gamma_N^{q\bar{q}} \quad (2.4)$$

and assume that both  $\gamma_N^{qq}$  and  $\gamma_N^{q\bar{q}}$  admit an analytic continuation for all values of  $N$  (as may be verified explicitly in perturbation theory[11]), it follows that the evolution equations (2.2) also admit a continuation for all values of  $N$ , such that  $q_N^\pm$  evolve multiplicatively according to

$$q_N^\pm(t) = \Delta_N^\pm(t, t_0) q_N^\pm(t_0), \quad (2.5)$$

where  $\Delta_N^\pm(t, t_0)$  are defined in terms of the anomalous dimensions

$$\gamma_N^\pm(t) = \gamma_N^{qq}(t) \pm \gamma_N^{q\bar{q}}(t). \quad (2.6)$$

In particular, the Gottfried sum evolves multiplicatively as

$$S_G(Q^2) = \Delta_1^+(t, t_0) S_G(Q_0^2). \quad (2.7)$$

This somewhat formal result becomes more transparent in the parton model, where the evolution of the quark distributions is found by using the Altarelli–Parisi equations[6]

$$\begin{aligned} \frac{d}{dt} q_i &= \sum_j \mathcal{P}_{q_i q_j} \otimes q_j + \sum_j \mathcal{P}_{q_i \bar{q}_j} \otimes \bar{q}_j + \mathcal{P}_{q_i G} \otimes G, \\ \frac{d}{dt} \bar{q}_i &= \sum_j \mathcal{P}_{\bar{q}_i \bar{q}_j} \otimes \bar{q}_j + \sum_j \mathcal{P}_{\bar{q}_i q_j} \otimes q_j + \mathcal{P}_{\bar{q}_i G} \otimes G, \end{aligned} \quad (2.8)$$



where  $\mathcal{P}$  are splitting functions, the sum runs over flavors, and  $\mathcal{P} \otimes q \equiv \int_x^1 \frac{dy}{y} \mathcal{P}(\frac{x}{y}) q(y)$ . Since, by charge conjugation,  $\mathcal{P}_{q_i q_j} = \mathcal{P}_{\bar{q}_i \bar{q}_j}$  and  $\mathcal{P}_{q_i \bar{q}_j} = \mathcal{P}_{\bar{q}_i q_j}$ , if we assume all relevant flavors to be massless there are only four distinct quark–quark or quark–antiquark splitting functions, namely  $\mathcal{P}_{qq}^D, \mathcal{P}_{q\bar{q}}^D, \mathcal{P}_{qq}^{ND}$  and  $\mathcal{P}_{q\bar{q}}^{ND}$ , where  $\mathcal{P}^D$  ( $\mathcal{P}^{ND}$ ) is any  $\mathcal{P}_{ij}$  such that  $i = j$  ( $i \neq j$ ). The evolution of the nonsinglet quark and antiquark distributions (1.5) is then simply given by

$$\begin{aligned} \frac{d}{dt} q &= \mathcal{Q}_{qq} \otimes q + \mathcal{Q}_{q\bar{q}} \otimes \bar{q}, \\ \frac{d}{dt} \bar{q} &= \mathcal{Q}_{q\bar{q}} \otimes \bar{q} + \mathcal{Q}_{qq} \otimes q; \\ \mathcal{Q} &= \mathcal{P}^D - \mathcal{P}^{ND}. \end{aligned} \tag{2.9}$$

This shows immediately that the eigenstates of the Altarelli–Parisi evolution are  $q^\pm$ , eqn.(2.1), since

$$\frac{d}{dt} q^\pm = (\mathcal{Q}_{qq} \pm \mathcal{Q}_{q\bar{q}}) \otimes q^\pm. \tag{2.10}$$

Taking moments of this equation and comparing the result with (2.5)-(2.6) it is clear that the anomalous dimensions  $\gamma_N^\pm$  (2.4) are just the  $N$ -th moments of the evolution kernel on the right hand side of eqn.(2.10), whereas  $\gamma_N^{qq}$  ( $\gamma_N^{q\bar{q}}$ ) are the  $N$ -th moments of  $\mathcal{Q}_{qq}$  ( $\mathcal{Q}_{q\bar{q}}$ ); this may be confirmed in perturbation theory by explicit computation. In particular, the nonsinglet evolution of  $F_2$  (and hence that of the Gottfried sum) is found by taking moments of  $\mathcal{Q}_{qq} + \mathcal{Q}_{q\bar{q}}$ .

In the parton model several useful perturbative properties of the anomalous dimensions  $\gamma_N^\pm$  become immediately apparent. Firstly, at one loop there is only one diagram which may contribute to nonsinglet evolution, namely gluon radiation by a quark line. Hence all the splitting functions  $\mathcal{P}_{q\bar{q}}$  vanish. On the other hand, at two loops the splitting functions  $\mathcal{P}_{q\bar{q}}^D$  and  $\mathcal{P}_{q\bar{q}}^{ND}$  do not vanish, since a quark may radiate a gluon which in turns radiates a  $q\bar{q}$  pair (see fig. 1). Furthermore the splitting functions  $\mathcal{P}_{q\bar{q}}^D$  and  $\mathcal{P}_{q\bar{q}}^{ND}$  are in general different already at two loops: the cross sections for flavor–diagonal and flavor–non-diagonal production differ since in the flavor diagonal case there are two identical particles in the final state, which must be antisymmetrized. It follows that all the  $\gamma_N^{q\bar{q}}$  start at two loops. Furthermore, specializing to the first moment, charge conservation implies that the first moment of  $q^-$  must be conserved (and thus that the Adler sum (1.6) does not evolve). It follows that  $\gamma_1^{qq} = \gamma_1^{q\bar{q}}$ , and in particular that they both vanish at one loop.

In conclusion, we see that in perturbative QCD the evolution of the Gottfried sum is governed by the anomalous dimension  $\gamma_1^+ = 2\gamma_1^{qq}$ , which is the first moment of the splitting functions for diagonal minus non-diagonal emission. This quantity starts at two loops, thus leading to a perturbative contribution to the evolution factor of the form

$$(\Delta_1^+)_{\text{pert}}(t, t_0) = 1 + \frac{\gamma_1^{+(2)}}{b^{(1)}} (\alpha_s(t) - \alpha_s(t_0)) + \dots \quad (2.11)$$

where  $\gamma_1^{+(2)}$  is the two-loop coefficient in  $\gamma_1^+$ , and  $b^{(1)}$  is the one-loop coefficient in the beta function. Explicit computation shows that[11]  $\gamma_1^{+(2)}/b^{(1)} \simeq 0.01$ ; as mentioned in the introduction the perturbative evolution is thus entirely negligible unless  $\alpha_s$  is so large that perturbation theory is useless.

This result was derived in the flavor-symmetric, vanishing quark mass limit. In principle, it may be corrected by two different kinds of effects. Firstly, if current quark masses are taken into account, then the simple evolution equation (2.5) is corrected by flavor-violating terms. These are usually assumed to be negligible, in that mass effects should be suppressed by powers of  $m^2/Q^2$ , although they have never been determined explicitly. If one also admits the possibility of isospin violation, then  $S_G$  also contains a term proportional to the proton-neutron difference of singlet structure functions, and the evolution of these must also be taken into account;  $S_G$  will then no longer evolve multiplicatively. This effect has been discussed in ref.[9], and is negligible for realistic amounts of isospin violation. We will neglect both these effects henceforth and assume isospin symmetry to be exact.

### 3. Evolution by Bound State Emission

The physical reason for the smallness of the perturbative evolution found in the previous section should be readily apparent: if we were to neglect final-state antisymmetrization effects, then the interaction which governs the QCD evolution would be fully symmetric under the  $U(N_f)$  flavor group, and the Wigner-Eckart theorem would imply that  $\mathcal{P}^D = \mathcal{P}^{ND}$ . There would then be no nonsinglet evolution, and the dynamically generated sea would be flavor symmetric, as naively expected. Final-state antisymmetrization effects spoil this argument, and provide a (tiny) dynamical violation of the flavor symmetry.

However, a much larger violation appears if we take into account[19] that in QCD the  $U(N_f)$  flavor symmetry is dynamically broken due to the axial anomaly[22]. In particular,

consider diagrams where a quark couples directly to a  $q\bar{q}$  bound state (fig. 2). We may view these as generated dynamically from diagrams which have the structure of the perturbative ones of fig. 1, but where the emitted (and unobserved) quark–antiquark pair may interact non–perturbatively. These diagrams will be suppressed at large scales where, due to the extended nature of the emitted bound states, they must lead to higher–twist contributions to the evolution equations — contributions suppressed by powers of  $1/Q^2$  in the large  $Q^2$  limit. However at low enough scales their contribution to nonsinglet evolution will probably be much greater than the perturbative diagrams. At very low scales it is no longer clear that the Altarelli–Parisi evolution picture is applicable at all. There might nevertheless be an intermediate region where the Altarelli–Parisi picture applies and the evolution due to bound–state emission is significant.

First, consider the situation in the chiral limit, with  $N_f$  massless quarks. Then, it is clear that all of the bound state emission diagrams will respect  $U(N_f)$  flavor symmetry, and thus will not contribute to nonsinglet evolution, with the sole exception of those in which pseudoscalar mesons are emitted. This is because it is only in the spectrum of pseudoscalar mesons that  $U(N_f)$  is broken down to  $SU(N_f)$  by non–perturbative effects coupled through the axial anomaly[22]; the  $N_f^2 - 1$  Goldstone bosons will make a significant contribution to nonsinglet evolution which is not cancelled off by the contribution of the singlet pseudoscalar (the  $\eta_0$ ) since this is kinematically suppressed. Away from the chiral limit, the emission of other mesons will also begin to contribute, but their contributions will remain relatively small mainly because the mass splittings are themselves relatively small, but also because they are in any case kinematically suppressed when compared to those of the light pseudoscalars. It follows that if we concentrate on nonsinglet evolution, then of the infinite tower of diagrams for bound–state emission (fig. 2) only those corresponding to pseudoscalar meson emission need be considered.

To make this discussion more quantitative consider the inclusion of pseudoscalar bound states  $\Pi^a$  in the evolution equation (2.8). We now have (omitting gluon contributions for simplicity)

$$\begin{aligned}
\frac{d}{dt}q_i &= \sum_j \mathcal{P}_{q_i q_j} \otimes q_j + \sum_j \mathcal{P}_{q_i \bar{q}_j} \otimes q_j + \sum_a \mathcal{P}_{q_i \Pi^a} \otimes \Pi^a, \\
\frac{d}{dt}\bar{q}_i &= \sum_j \mathcal{P}_{\bar{q}_i \bar{q}_j} \otimes \bar{q}_j + \sum_j \mathcal{P}_{\bar{q}_i q_j} \otimes q_j + \sum_a \mathcal{P}_{\bar{q}_i \Pi^a} \otimes \Pi^a, \\
\frac{d}{dt}\Pi^a &= \sum_j \mathcal{P}_{\Pi^a q_j} \otimes q_j + \sum_j \mathcal{P}_{\Pi^a \bar{q}_j} \otimes \bar{q}_j + \sum_b \mathcal{P}_{\Pi^a \Pi^b} \otimes \Pi^b,
\end{aligned} \tag{3.1}$$

where  $\Pi^a(x; t)$  are the distribution functions of the pseudoscalar mesons (the pion octet and the  $\eta'$ ). The first two equations in (3.1) express the evolution of the quark and antiquark distribution due to pseudoscalar emission, whereas the last equation gives the evolution of the pseudoscalar meson distribution. The former is determined by the splitting functions  $\mathcal{P}_{qq}$ , which expresses the probability of a quark to be emitted by another quark (with emission of an unobserved pseudoscalar), and  $\mathcal{P}_{q\Pi}$ , which expresses the probability of a pseudoscalar to fragment into a quark and an antiquark (one of which is observed). The latter is determined by the splitting functions  $\mathcal{P}_{\Pi q}$  and  $\mathcal{P}_{\Pi\Pi}$ , which give the probability of a pseudoscalar to be emitted by a quark or another pseudoscalar, respectively.

Isospin and charge conjugation invariance imply that for neutral pseudoscalars  $\Pi^0 \equiv (\pi^0, \eta, \eta')$

$$\mathcal{P}_{u\Pi^0} = \mathcal{P}_{d\Pi^0} = \mathcal{P}_{\bar{u}\Pi^0} = \mathcal{P}_{\bar{d}\Pi^0}, \quad (3.2)$$

whereas for charged mesons

$$\begin{aligned} \mathcal{P}_{u\pi^+} &= \mathcal{P}_{d\pi^-} = \mathcal{P}_{\bar{d}\pi^+} = \mathcal{P}_{\bar{u}\pi^-} \equiv \mathcal{P}_{q\pi}, \\ \mathcal{P}_{d\pi^+} &= \mathcal{P}_{u\pi^-} = \mathcal{P}_{\bar{u}\pi^+} = \mathcal{P}_{\bar{d}\pi^-} = 0. \end{aligned} \quad (3.3)$$

The non-perturbative evolution of the nonsinglet quark and antiquark distributions (1.5) and the pion distribution

$$\pi(x; t) \equiv \pi^+(x; t) - \pi^-(x; t), \quad (3.4)$$

is thus given by

$$\begin{aligned} \frac{d}{dt}q &= \mathcal{Q}_{qq} \otimes q + \mathcal{Q}_{q\bar{q}} \otimes \bar{q} + \mathcal{P}_{q\pi} \otimes \pi, \\ \frac{d}{dt}\bar{q} &= \mathcal{Q}_{q\bar{q}} \otimes \bar{q} + \mathcal{Q}_{q\bar{q}} \otimes q - \mathcal{P}_{q\pi} \otimes \pi, \\ \frac{d}{dt}\pi &= \mathcal{P}_{\pi q} \otimes (q - \bar{q}) + \mathcal{P}_{\pi\pi} \otimes \pi. \end{aligned} \quad (3.5)$$

The combinations  $q^\pm$  (2.1) then satisfy

$$\begin{aligned} \frac{d}{dt}q^+ &= (\mathcal{Q}_{qq} + \mathcal{Q}_{q\bar{q}}) \otimes q^+, \\ \frac{d}{dt}q^- &= (\mathcal{Q}_{q\bar{q}} - \mathcal{Q}_{q\bar{q}}) \otimes q^- + \mathcal{P}_{q\pi} \otimes 2\pi, \\ \frac{d}{dt}\pi &= \mathcal{P}_{\pi q} \otimes q^- + \mathcal{P}_{\pi\pi} \otimes \pi, \end{aligned} \quad (3.6)$$

where, to first order, only the splitting functions  $\mathcal{P}_{qq} = \mathcal{P}_{q\bar{q}}$ ,  $\mathcal{P}_{q\Pi}$ ,  $\mathcal{P}_{\bar{q}\Pi}$ ,  $\mathcal{P}_{\Pi q}$  and  $\mathcal{P}_{\Pi\bar{q}}$  are nonvanishing<sup>3</sup> (and in particular  $\mathcal{Q}_{q\bar{q}} = 0$ ).

To actually compute the nonsinglet evolution due to pseudoscalar meson emission, we use the probabilistic interpretation[26] of the Altarelli–Parisi equations in which the splitting functions  $\mathcal{P}_{qq}$  are obtained through the same sort of procedure which leads to the perturbative splitting functions[6]. That is, QCD evolution is in general due to the fact that in deep inelastic scattering a parton may radiate another particle (perturbatively a gluon, but for present purposes a pseudoscalar bound state,  $\Pi$ ) either before or after it is struck by the virtual photon. The splitting function  $\mathcal{P}_{q_i q_j}(x)$  expresses the probability of the quark parton  $q_j$  to carry the fraction  $x$  momentum of the quark parton  $q_i$  after the radiation process, and it may be obtained from the cross-section for Compton-like scattering of a (virtual) photon  $\gamma^*$  before or after emission of a bound state (fig. 3). This corresponds to an effective resummation of the same ladder diagrams which lead to the usual Altarelli–Parisi evolution, with the exchanged gluons replaced by pseudoscalar mesons. These diagrams may be shown to give the dominant contribution in the leading logarithmic approximation in a theory where quarks are coupled to pointlike pseudoscalar particles in just the same way as for perturbative QCD, but without the complications arising from gauge invariance [27,28]. In section 4 we will discuss the applicability of this picture to extended pseudoscalars.

The contribution of the emission of a bound state  $\Pi$  to the splitting function  $\mathcal{P}_{q_i q_j}$  is then given by

$$[\mathcal{P}_{q_i q_j}(x; t)]_{\Pi} = \frac{d}{dt} \sigma_{q_i q_j}^{\gamma^* \Pi}(x; t), \quad (3.7)$$

where  $\sigma_{q_i q_j}^{\gamma^* \Pi}(x; t)$  is the total cross section for emission of the state  $\Pi$  with quantum numbers corresponding to the given splitting function, expressed in terms of the usual scaling variables and integrated over all  $k_{\perp}$ . This cross-section is adimensional, due to the extraction of a scale factor[6]. Notice that the so-called “loss” terms[6,26], namely those terms which give the decrease in the probability of finding a quark with momentum fraction  $x$  due to the fact that if such a quark undergoes a radiation process it is lost from the observed momentum interval, are absent from eqn.(3.7), which gives the full splitting

---

<sup>3</sup>  $\mathcal{P}_{\Pi\Pi}$  begins at second order (just as the usual perturbative contributions to  $\mathcal{P}_{qq}$  only begin at second order), while although  $\mathcal{P}_{q\bar{q}}$  may receive nontrivial contributions from diquark emission, the  $U(N_f)$  symmetry of the diquark is not broken anomalously, and thus they may be ignored for the same reason as we ignore the contribution of all mesons other than pseudoscalars to  $\mathcal{P}_{qq}$ .

function. This is because when a meson is emitted the quark which is struck by the virtual photon is never the same as the original one, even if it has the same flavor.

The non-perturbative contribution to the anomalous dimension  $\gamma_N^{q_i q_j}$  is then found by taking moments of the splitting function:

$$[\gamma_N^{q_i q_j}(t)]_\Pi = \int_0^{x_{\max}} dx x^{N-1} [\mathcal{P}_{q_i q_j}(x; t)]_\Pi = \frac{d}{dt} \int_0^{x_{\max}} dx x^{N-1} \sigma_{q_i q_j}^{\gamma^* \Pi}(x; t). \quad (3.8)$$

Notice that the upper limit of the  $x$ -integration is not 1 but rather

$$x_{\max} = \frac{1}{1 + \frac{M^2}{Q^2}} \leq 1, \quad (3.9)$$

where  $M$  is the mass of the pseudoscalar bound state. The cross-section vanishes for  $x > x_{\max}$ . By continuity we also expect  $\sigma_{q_i q_j}^{\gamma^* \Pi}(x_{\max}; t) = 0$ ; this justifies the exchange in the order of differentiation and integration in the second expression (3.8). The anomalous dimensions  $\gamma_N^{q\Pi}$  and  $\gamma_N^{\Pi q}$  are similarly determined by taking moments of the splitting functions  $\mathcal{P}_{q\Pi}$  and  $\mathcal{P}_{\Pi q}$  obtained by differentiating the cross-sections  $\sigma_{q\Pi}$  and  $\sigma_{\Pi q}$ .

Besides the usual crossing symmetry relations among splitting functions [6], charge conservation as expressed by the Adler sum rule eqn.(1.6) imposes a nontrivial consistency condition on the first moments of the various splitting functions. Combining (1.6) with the evolution equation (3.6) and taking the first moment gives

$$\gamma_1^{qq}(t) + 2\gamma_1^{q\pi}(t)\pi_1(t) = 0, \quad (3.10)$$

where  $\gamma_1^{qq}$  is the first moment of  $\mathcal{Q}_{qq}$ , and  $q_1(t)$  and  $\pi_1(t)$  are the first moments of  $q(x; t)$  and  $\pi(x; t)$  respectively. If we now assume that there exists a scale  $t_0$  such that  $\pi_1(t_0) = 0$ , the entire pion distribution  $\pi(x; t)$  is generated dynamically through the relevant evolution equation (3.6). Integrating up the first moment of this evolution, and using the result in eqn.(3.10) leads to the condition

$$\gamma_1^{qq}(t) + 2\gamma_1^{q\pi}(t) [\sigma_{\pi q}^1(t) - \sigma_{\pi q}^1(t_0)] = 0, \quad (3.11)$$

where  $\sigma_{\pi q}^1$  is the first moment of the appropriate cross-section, so that  $\gamma_1^{\pi q}(t) = \frac{d}{dt} \sigma_{\pi q}^1$ . Now eqn.(3.11) means that  $\gamma_1^{qq}(t_0) = 0$ ; the assumption that  $\pi_1(t)$  is entirely generated by the evolution eqn.(3.6) is consistent only if the evolution of  $q_1(t)$  flattens at small  $t$ . The scale  $t_0$  at which the evolution flattens is then the same as that where  $\pi_1(t)$  vanishes.

In this formalism the so-called Sullivan process[29], where the virtual photon scatters inelastically on the quarks in a pion which is in turn carrying a fraction of the nucleon momentum, is regarded as a measurement of the  $\Pi^a(x)$  structure functions through their fragmentation into quark-antiquark pairs, as described by the splitting function  $\mathcal{P}_{q\Pi}$ . This is the nonperturbative analogue, for pseudoscalar bound states, of a perturbative measurement of the gluon distribution via photon-gluon fusion. Because some of the bound states we consider are charged, there is also the possibility of a direct coupling of the virtual photon to these states, corresponding to processes where the pion does not fragment incoherently, but rather is viewed as a pointlike effective constituent. Such processes, however, are suppressed by the square of the pion form factor, evaluated at the photon's virtuality  $Q^2$ , and are thus negligible [29]. Furthermore they are only relevant to the evolution of singlet structure functions; for nonsinglets, and in particular for the Gottfried sum, they vanish identically because of isospin.

Eqns (3.1)-(3.7) provide us thus with a well-defined framework in which to calculate nonperturbative contributions to the evolution of structure functions due to the inclusion of pseudoscalar mesons as effective constituents in the ladder diagrams which lead to Altarelli-Parisi evolution. In order to avoid double counting, the non-perturbative contribution to the anomalous dimensions determined in this way should not be added directly to the usual perturbative anomalous dimensions. Rather, the non-perturbative contribution, while dominant at small  $Q^2$ , must fall as a power at large  $Q^2$ , eventually falling below the logarithmic perturbative evolution. At around this point (which would ideally be in a region where both calculations can still be believed) the non-perturbative and perturbative anomalous dimensions should be matched together. In the particular case of the Gottfried sum the perturbative evolution eqn.(2.11) is so tiny that it may be ignored; the only significant evolution is nonperturbative.

We specialize now to the evolution of  $q^+(x; t)$ . It is apparent from eqn.(3.6) that the pion distribution  $\pi(x; t)$  makes no direct contribution to this evolution. This is to be expected [9] on the basis of a simple quark counting argument: because quarks and antiquarks contribute with the same sign to Gottfried sum eqn.(1.1),(1.3), it follows that any pion always give a vanishing contribution to  $S_G$  eqn.(1.1). The emission of bound states contributes nevertheless indirectly, by leading to nonperturbative evolution of  $q^+(x; t)$ . The evolution of the Gottfried sum discussed in the present approach thus appears to be due to a mechanism which is physically distinct from the Sullivan process; indeed, in the present

approach scattering on the pion component of the nucleon does not contribute at all to  $S_G$ , contrary to the suggestion in ref.[15]<sup>4</sup>.

The non-perturbative evolution of the  $N$ -th moment of the nonsinglet quark distributions  $q_N^+(x)$  (1.5),(2.1) is found by computing the anomalous dimensions (3.8) for the  $u$  and  $d$  flavors and the pseudoscalar mesons  $\pi^\pm$ ,  $\pi^0$ ,  $\eta$  and  $\eta'$ . For simplicity we may assume that the latter are pure octet and pure singlet, since the appropriate mixing angle  $\theta_P$  is small ( $\sin^2 \theta_P \simeq 0.1$ ). Noting that the probability for flavor-diagonal emission by a light quark is obtained by adding the probabilities for the process to go through  $\pi^0$ ,  $\eta$  and  $\eta'$  meson emission as dictated by their quark content we find

$$\begin{aligned}\gamma_N^{ud} &= \gamma_N^{du} = \frac{d}{dt} \sigma_N^{\gamma^* \pi^+} = \frac{d}{dt} \sigma_N^{\gamma^* \pi^-}, \\ \gamma_N^{uu} &= \gamma_N^{dd} = \frac{d}{dt} \left( \frac{1}{2} \sigma_N^{\gamma^* \pi^0} + \frac{1}{6} \sigma_N^{\gamma^* \eta} + \frac{1}{3} \sigma_N^{\gamma^* \eta'} \right), \\ \gamma_N^{us} &= \gamma_N^{su} = \frac{d}{dt} \sigma_N^{\gamma^* K^+} = \frac{d}{dt} \sigma_N^{\gamma^* K^-}, \\ \gamma_N^{ds} &= \gamma_N^{sd} = \frac{d}{dt} \sigma_N^{\gamma^* K^0} = \frac{d}{dt} \sigma_N^{\gamma^* \bar{K}^0}, \\ \gamma_N^{ss} &= \frac{d}{dt} \left( \frac{2}{3} \sigma_N^{\gamma^* \eta} + \frac{1}{3} \sigma_N^{\gamma^* \eta'} \right),\end{aligned}\tag{3.12}$$

where  $\sigma_N^{\gamma^* \Pi}$  is the  $N$ -th moment (defined as in the right hand side of eqn.(3.8)) of the cross section for the process of fig. 3, and we have included for completeness strange quarks and kaon emission. Using eqn.(3.12) in the evolution equation (3.6) we finally get

$$\begin{aligned}\gamma_N^+ &= \gamma_N^{qq} = \gamma_N^{uu} - \gamma_N^{ud} = \frac{d}{dt} \left( \frac{1}{2} \sigma_N^{\gamma^* \pi^0} + \frac{1}{6} \sigma_N^{\gamma^* \eta} + \frac{1}{3} \sigma_N^{\gamma^* \eta'} - \sigma_N^{\gamma^* \pi^+} \right) \\ &\simeq \frac{d}{dt} \left( \frac{1}{6} \sigma_N^{\gamma^* \eta} + \frac{1}{3} \sigma_N^{\gamma^* \eta'} - \frac{1}{2} \sigma_N^{\gamma^* \pi} \right).\end{aligned}\tag{3.13}$$

The non-perturbative contribution to the evolution factor for the Gottfried sum (2.7) is thus

$$\begin{aligned}[\Delta_1^+(t, t_0)]_{\text{nonpert}} &= \exp \left( \left[ \frac{1}{6} \sigma_1^{\gamma^* \eta'}(t) + \frac{1}{3} \sigma_1^{\gamma^* \eta'}(t) - \frac{1}{2} \sigma_1^{\gamma^* \pi}(t) \right] \right. \\ &\quad \left. - \left[ \frac{1}{6} \sigma_1^{\gamma^* \eta'}(t_0) + \frac{1}{3} \sigma_1^{\gamma^* \eta'}(t_0) - \frac{1}{2} \sigma_1^{\gamma^* \pi}(t_0) \right] \right).\end{aligned}\tag{3.14}$$

---

<sup>4</sup> Notice however that in some specific low energy models the Sullivan process is actually related[14] by the dynamics of the pion radiation mechanism to the distribution of quarks in the recoil hadron after pion emission, thus it may contribute indirectly to quark distributions in a way which is analogous to that which we discuss here. In these models, however, there is no scale dependence of structure functions and quark distributions.



Whereas the perturbative evolution (2.11) was very small the non-perturbative scale factor (3.14) is potentially large. In particular, the role played by the anomalous  $U(N_f)$  symmetry breaking in the pseudoscalar spectrum is now apparent: because of the large  $\eta$ - $\pi$  and  $\eta'$ - $\pi$  mass differences we expect the corresponding emission cross sections to be significantly different. In the  $U(N_f)$ -symmetric limit all cross sections would be the same and the right hand side of eqn.(3.13), and thus the exponent in eqn.(3.14), would be identically equal to zero. In reality, whereas for very large values of  $Q^2$  the effects of the pseudoscalar mesons' masses should be negligible and the non-perturbative scale factor should flatten (as  $1/Q^2$ ), for scales of the order of the nucleon mass the effects of the mass splitting will be so large that the  $\eta$  and  $\eta'$  production cross sections will be negligible when compared to that of the  $\pi$ . Thus because of the axial anomaly the diagonal radiation process is disfavoured compared to the non-diagonal one, as half of it proceeds through  $\eta$  and  $\eta'$  emission, which is dynamically suppressed. So not only is the evolution purely multiplicative, but since the cross-sections are all positive, it necessarily results in the screening of the Gottfried sum; eqn.(3.14) shows that  $S_G$  is always reduced as  $Q^2$  is increased.

In order to make these observations quantitative, we must proceed to the computation of the various radiation cross sections and the determination of their first moment. We will do this in the next section.

#### 4. Non-perturbative Splitting Functions

The computation of the non-perturbative splitting function reduces to the computation of the cross section for the process  $\gamma^*q \rightarrow \Pi q$ , where  $\Pi$  is a pseudoscalar meson, which at leading order is given by the two diagrams displayed in fig. 3. In order to perform this computation we must introduce an effective quark-pseudoscalar coupling. Writing the quark propagator as  $S^{-1}(p) = (\not{p} + \Sigma(p^2))^{-1}$ , where  $\Sigma(p^2)$  is the quark self energy, the most general such coupling is, by definition,

$$\chi(k, p) \equiv S^{-1}(p + \tfrac{1}{2}k) \langle 0 | \psi(p - \tfrac{1}{2}k) \bar{\psi}(p + \tfrac{1}{2}k) | \Pi(k) \rangle S^{-1}(p - \tfrac{1}{2}k), \quad (4.1)$$

where  $|\Pi(k)\rangle$  is the meson state, and the momenta are notated as in fig. 2. The quark dynamics may thus be summarized by writing an effective action

$$S_{\text{eff}} = \int d^4p \bar{\psi}(p) i \not{D} \psi(p) + \int d^4p \int d^4k \bar{\psi}(p + \tfrac{1}{2}k) f \chi(k, p) U(k) \psi(p - \tfrac{1}{2}k), \quad (4.2)$$

where  $U(k) \equiv \exp(i\gamma_5 \Pi(k)/f_\Pi)$  is a nonlinear representation of the pseudoscalar field  $\Pi(k)$ ; expanding  $U$  in powers of  $\Pi$  gives the quark self energy and then couplings of the  $q\bar{q}$  pair to increasing numbers of pseudoscalars  $\Pi$ . In the chiral limit (i.e. ignoring quark masses) the quark self-energy and the on-shell coupling to pions are thus related by the chiral Ward–Takahashi identity

$$\Sigma(p) = f\chi(0, p), \quad (4.3)$$

$f$  being the meson decay constant (see for example [30]). Effective actions such as eqn.(4.2) have long been used to discuss dynamical chiral symmetry breaking and to compute meson form factors and decay amplitudes [31–33]; more recently attempts have been made to find a formal justification for them within QCD ([34] and references therein) and to develop their low energy phenomenological implications more systematically [35].

The effective coupling (4.1) may be expanded in terms of a set of four scalar vertex functions  $\phi_i(k, p)$ ,  $i = 0, 1, 2, 3$ ;

$$\chi(k, p) = \phi_0(k, p) + \phi_1(k, p)\not{k} + \phi_2(k, p)(k \cdot p)\not{p} + \phi_3(k, p)\frac{1}{2}(\not{p}\not{k} - \not{k}\not{p}). \quad (4.4)$$

The vertex functions are all even functions of  $k \cdot p$ , and for on-shell pseudoscalars we may expand them as

$$\phi_i(k, p) = \sum_{n=0}^{\infty} \phi_i^n(p^2)(k \cdot p)^{2n}. \quad (4.5)$$

Now, in principle, all of the on-shell vertex functions  $\phi_i^n(p)$  may be computed by solving the homogeneous bound state equation, separated out into a hierarchy of equations corresponding to increasing powers of  $k$ . In practice of course this is not possible since the quark–antiquark scattering kernel is unknown except at large Euclidean momentum transfer. The asymptotic behaviour for large Euclidean  $p^2$  is given by[36]

$$\begin{aligned} \phi_0^n(p^2) &\underset{p^2 \rightarrow \infty}{\sim} \frac{(\log p^2)^{\delta_0^n}}{(p^2)^{n+1}}, \\ \phi_1^n(p^2) &\underset{p^2 \rightarrow \infty}{\sim} p^2 \phi_2^n(p^2) \underset{p^2 \rightarrow \infty}{\sim} \frac{(\log p^2)^{\delta_1^n}}{(p^2)^{n+1}}, \quad \phi_3^n(p^2) \underset{p^2 \rightarrow \infty}{\sim} \frac{(\log p^2)^{\delta_3^n}}{(p^2)^{n+2}}, \end{aligned} \quad (4.6)$$

where the numbers  $\delta_i^n$  are related to the anomalous dimensions of various local operators, and decrease monotonically in  $n$ . Asymptotically, the dominant vertices are thus  $\phi_i(p^2) \equiv \phi_i^0(p^2)$  for  $i = 0, 1, 2$ . Furthermore, it can be seen from examination of the bound state equations that all the  $\phi_i^n(p^2)$  remain finite as  $p^2 \rightarrow 0$ .

The normalization of the vertex functions is fixed by the chiral Ward–Takahashi identity (4.3) in terms of the self–energy and  $f_\pi$ :

$$\phi_0^\pi(p^2) = \Sigma(p^2)/f_\pi. \quad (4.7)$$

The scale of  $\Sigma(p^2)$ , in turn, is in principle given by solution of the (nonlinear) Schwinger–Dyson equation in terms of  $\Lambda_{QCD}$ . Infrared uncertainties make such a determination unrealistic, however[36], and it is more practical to use the Pagels–Stokar condition[33] which normalizes  $\Sigma(p^2)$  to the pion decay constant  $f_\pi = 93$  MeV:

$$f_\pi^2 = \frac{N_c}{4\pi^2} \int_0^\infty dp^2 p^2 \Sigma(p^2) \frac{\Sigma(p^2) - \frac{1}{2}p^2 \frac{d\Sigma(p^2)}{dp^2}}{(p^2 + \Sigma(p^2)^2)^2}. \quad (4.8)$$

Then, using eqn.(4.7) in eqn.(4.8) fixes the strength of the meson–quark coupling, or (more precisely) the normalization of the vertex function in terms of the scale of the quark self–energy. A consistency check on the condition (4.8) can be obtained by considering the asymptotic behaviour of the pion electromagnetic form factor (also derived in ref.[33]):

$$Q^2 F_\pi(Q^2) \underset{Q^2 \rightarrow \infty}{\sim} \frac{N_c \ln 2}{4\pi^2 f_\pi^2} \int_0^\infty dp^2 p^2 \frac{\Sigma(p^2)^2}{(p^2 + \Sigma(p^2)^2)^2}. \quad (4.9)$$

In principle all the other vertex functions may now be found using the homogeneous Bethe–Salpeter equations without the need for further normalization conditions, though in practice this is again not really viable since they are too sensitive to the unknown infrared dynamics.

It is now straightforward to compute the spin–averaged cross section corresponding to the two diagrams of fig. 3. Assuming that all the quark partons are massless, writing  $M$  for the mass of the emitted meson, and  $-Q^2$  for the virtuality of the incident photon, the usual Mandelstam invariants  $\hat{s}$ ,  $\hat{t}$ ,  $\hat{u}$ , are given, in terms of the four external particles’ four–momenta indicated in fig. 3, by

$$\begin{aligned} \hat{s} &= (p_i + q)^2 = (p_f + k)^2 = -Q^2 + 2p_i \cdot q = M^2 + 2p_f \cdot k, \\ \hat{t} &= (p_i - k)^2 = (p_f - q)^2 = -Q^2 - 2p_f \cdot q = M^2 - 2p_i \cdot k, \\ \hat{u} &= (p_i - p_f)^2 = (q - k)^2 = -2p_i \cdot p_f = M^2 - Q^2 - \hat{s} - \hat{t}. \end{aligned} \quad (4.10)$$

The physical kinematical region is  $\hat{s} \geq M^2$ ,  $\hat{t} \leq 0$ ,  $\hat{u} \leq 0$ . Introducing the appropriate kinematical factors<sup>5</sup> then, after a lengthy computation, the cross section reduces to the relatively simple form

$$\sigma_{qq}^{\gamma^*\Pi}(\hat{s}, \hat{t}) = -\frac{1}{16\pi^2} \left[ \varphi_{\hat{s}}^2 \left( \frac{\hat{t}}{\hat{s}} + \frac{Q^2 M^2}{\hat{s}^2} \right) + \varphi_{\hat{t}}^2 \left( \frac{\hat{s}}{\hat{t}} + \frac{Q^2 M^2}{\hat{t}^2} \right) + 2\varphi_{\hat{s}}\varphi_{\hat{t}} \left( 1 - \frac{M^2}{\hat{s}} \right) \left( 1 - \frac{M^2}{\hat{t}} \right) + (\tilde{\varphi}_{\hat{s}} - \tilde{\varphi}_{\hat{t}})^2 \hat{u} \right], \quad (4.11)$$

where

$$\begin{aligned} \varphi_{\hat{s}} &\equiv \sum_{n=0}^{\infty} \left( \frac{1}{2} \hat{s} \right)^{2n} \left[ \phi_0^n \left( \frac{1}{4} (2\hat{s} - M^2) \right) + \frac{1}{2} (\hat{s} - M^2) \phi_3^n \left( \frac{1}{4} (2\hat{s} - M^2) \right) \right], \\ \tilde{\varphi}_{\hat{s}} &\equiv \sum_{n=0}^{\infty} \left( \frac{1}{2} \hat{s} \right)^{2n} \left[ \phi_1^n \left( \frac{1}{4} (2\hat{s} - M^2) \right) + \frac{1}{4} \hat{s} \phi_2^n \left( \frac{1}{4} (2\hat{s} - M^2) \right) \right], \end{aligned} \quad (4.12)$$

and similarly for  $\varphi_{\hat{t}}$  and  $\tilde{\varphi}_{\hat{t}}$ .

The cross section in terms of scaling variables is obtained by expressing the Mandelstam invariants in terms of  $x$ ,  $Q^2$ , and the center-of-mass scattering angle  $\theta$ . In the limit of vanishing quark mass (but retaining of course the meson's mass) we have

$$\begin{aligned} \hat{s} &= \frac{1-x}{x} Q^2, \\ \hat{t} &= -\frac{(1-x)Q^2 - xM^2}{2x(1-x)} (1 - \cos \theta) - \frac{xM^2}{1-x}, \\ \hat{u} &= -\frac{(1-x)Q^2 - xM^2}{2x(1-x)} (1 + \cos \theta). \end{aligned} \quad (4.13)$$

The physical region corresponds thus to  $0 \leq x \leq x_{\max}$ , with  $x_{\max}$  given by eqn.(3.9). It is now easy to check that when  $x = x_{\max}$ ,  $\hat{s} = M^2$ ,  $\hat{t} = -Q^2$  and  $\hat{u} = 0$ , so  $\sigma_{qq}^{\gamma^*\Pi}$  vanishes identically, as we claimed following eqn.(3.8). Integrating  $\sigma_{qq}^{\gamma^*\Pi}(\hat{s}, \hat{t})$  over  $\cos \theta$  from  $-1$  to  $1$  then gives the cross-section  $\sigma_{qq}^{\gamma^*\Pi}(x; \ln Q^2)$  which enters the expression (3.8) for the anomalous dimensions, and thus (3.14) for the evolution of the Gottfried sum.

---

<sup>5</sup> The cross section is dimensionless after the extraction of a scale factor which we fix in such a way that in the limit in which the meson is point-like the canonically normalized splitting function [6] for emission of scalar particles is reproduced.

Before we can do this, however, we must decide on a particular form for the vertex functions. From the asymptotic behaviour (4.6), and the definitions (4.12) we may infer that

$$\varphi_{\hat{s}} \underset{\hat{s} \rightarrow \infty}{\sim} \frac{(\log \hat{s})^{\delta_0^0}}{\hat{s}}, \quad \tilde{\varphi}_{\hat{s}} \underset{\hat{s} \rightarrow \infty}{\sim} \frac{(\log \hat{s})^{\delta_1^0}}{\hat{s}}; \quad (4.14)$$

we also know that both remain finite at small  $\hat{s}$ . We use these facts to justify the simple ansätze<sup>6</sup>  $\varphi_{\hat{s}} = \varphi(\frac{1}{4}(2\hat{s} - M^2))$ ,  $\varphi_{\hat{t}} = \varphi(\frac{1}{4}(M^2 - 2\hat{t}))$  with

$$\varphi^\pi(p^2) = \frac{m_d}{f_\pi} \frac{\Lambda^2 + m_d^2}{\Lambda^2 + p^2}, \quad \tilde{\varphi}^\pi(p^2) = \frac{g_\pi}{f_\pi} \frac{\tilde{\Lambda}^2 + m_d^2}{\tilde{\Lambda}^2 + p^2}. \quad (4.15)$$

Similar forms will be assumed for the  $\eta$  and  $\eta'$  vertex functions. We also make the simplifying assumption (strictly justifiable only asymptotically) that  $\Sigma(p^2) = f_\pi \varphi^\pi(p^2)$ .

The parameters  $\Lambda$  and  $\tilde{\Lambda}$  give the scale of transition of the vertex functions from the hard (pointlike) to the soft (extended) region; they may be thought of as parameterizing the “size” of the bound state. The normalization condition eqn.(4.8) fixes the strength of the pion–quark coupling by fixing  $m_d$  as a function of  $\Lambda$ . Because  $m_d$  may be identified with the dynamical quark mass (actually the “pole” mass, since  $\Sigma(m_d^2) = m_d$ )  $\Lambda$  could then be fixed by requiring this to be equal to the constituent quark mass. However, given the large uncertainty on this quantity, this only gives us a range of acceptable values of  $\Lambda$ , rather than fixing it completely. There is no comparable way of fixing  $g_\pi$ , so we must treat  $g_\pi$  and  $\tilde{\Lambda}$  as free parameters; the dependence of the cross–section(4.11) on these is however rather weak except in the large  $Q^2$  region, as we will see in detail below.

Eqn.(4.11) shows that the cross section is dominated by the region where either the  $t$ -channel or the  $s$ -channel<sup>7</sup> intermediate particle goes close to the mass shell (which it can never reach because of the meson mass) — the region where either  $\hat{t}$  or  $\hat{s}$  is small. Physically, this corresponds to the emitted meson and the quark being (almost) collinear in the respective diagrams fig. 3a and fig. 3b, consistent with the probabilistic interpretation. In this region the form factors eqn.(4.14) are essentially pointlike if the mesons are light. Now, eqn.(4.13) shows that in the  $t$ -channel this occurs when  $\theta = 0$  and  $x$  is small, whereas

---

<sup>6</sup> Even though the asymptotic behaviour (4.6) may only be proven rigorously for spacelike  $p^2 > 0$  we assume that it may be analytically continued to timelike  $p^2 < 0$ ; we will need vertex functions in both spacelike and timelike regions, since although  $\hat{s} > \frac{1}{2}M^2$ ,  $\hat{t} < \frac{1}{2}M^2$  (see (4.13)).

<sup>7</sup> The fact that the  $s$ -channel diagrams can also be resummed and factorized just as the  $t$ -channel ladder diagrams is discussed for a theory of scalar gluons in ref.[28].

in the  $s$ -channel it occurs when  $x$  is close to  $x_{\max}$  (as given by eqn.(3.9)). Both conditions are valid for all  $Q^2$ , even though the phase-space region (i.e., the  $x$ -range) where  $\hat{s}$  and  $\hat{t}$  are close to their respective minimal values gets smaller as  $Q^2$  increases.

This implies that for moderate  $Q^2$  the cross section eqn.(4.11) is not only significantly increasing with  $Q^2$ , but also it is dominated by the collinear region where the form factors are close to pointlike and the dominance of ladder diagrams is valid. As  $Q^2$  increases the cross-section increases more slowly. Even though the bulk of the cross section still comes from the collinear region, its growth is effectively cut by the extended tail of the form factor, thus leading to anomalous dimensions which have a “higher-twist” fall-off as inverse powers of  $Q^2$ , until eventually the nonperturbative cross-section is negligible as compared to the perturbative one. The cross-section (4.11) with form factors behaving asymptotically as (4.14) thus provides a smooth interpolation between the region where strong nonperturbative evolution takes place, and the asymptotic perturbative region<sup>8</sup>.

So far we have taken all the quarks to be massless; the resulting cross section (4.11) then diverges at small  $\hat{s}$  or small  $\hat{t}$ , and, as we discuss in the next section, this means that the evolution due to Goldstone bosons diverges in the chiral limit  $M \rightarrow 0$ . This is unacceptable, but easily cured. Since we have effectively included radiative corrections to the two-loop perturbative evolution diagram of fig. 2 which turn the emitted (and unobserved)  $q\bar{q}$  pair into a bound state (a meson) we should include also radiative corrections on the propagating quark<sup>9</sup>. Indeed, this is required for consistency: since we are treating the nonsinglet pseudoscalars as Goldstone bosons, which become massless in the chiral limit, chiral symmetry must have been broken dynamically, and the propagating quarks must have a dynamically generated self energy  $\Sigma(p^2)$  (as may be seen directly from eqn.(4.7)) of the order of several hundreds of MeV.

The quark self energy corrections can be absorbed into the vertex functions by the simple replacement

$$\chi(p_f + \tfrac{1}{2}k, k) \rightarrow \frac{\hat{s} - (\not{p}_i + \not{k})\Sigma(\hat{s})}{\hat{s} + \Sigma^2(\hat{s})}\chi(p_f + \tfrac{1}{2}k, k) \quad (4.16)$$

---

<sup>8</sup> If instead of (4.15) we were to take the cruder forms  $\varphi(p^2) = \theta(\Lambda^2 - p^2)$ ,  $\tilde{\varphi}(p^2) = 0$  we would, after a chiral rotation, recover the chiral quark model[20] as used in [19]. This is not an acceptable approximation precisely because it is the  $1/p^2$  fall-off of  $\varphi(p^2)$ , as embodied in (4.15), which gives the higher twist evolution at large  $Q^2$ .

<sup>9</sup> Though not of course on the external ones.

in the  $s$ -channel, and similarly for the  $t$ -channel. By rewriting these new amplitudes in the form (4.4), it is not difficult to see that the cross-section retains its simple form (4.11), but now with

$$\begin{aligned}\varphi_{\hat{s}} &\equiv \frac{\hat{s}}{\hat{s} + \Sigma^2(\hat{s})} \sum_{n=0}^{\infty} \left(\frac{1}{2}\hat{s}\right)^{2n} \left[\phi_0^n + \frac{1}{2}(\hat{s} - M^2)\phi_3^n + \left(\phi_1^n + \frac{1}{4}\hat{s}\phi_2^n\right)\Sigma(\hat{s})\right], \\ \tilde{\varphi}_{\hat{s}} &\equiv \frac{1}{\hat{s} + \Sigma^2(\hat{s})} \sum_{n=0}^{\infty} \left(\frac{1}{2}\hat{s}\right)^{2n} \left[\hat{s}(\phi_1^n + \frac{1}{4}\hat{s}\phi_2^n) + \left(\phi_0^n + \frac{1}{2}(\hat{s} - M^2)\phi_3^n\right)\Sigma(\hat{s})\right],\end{aligned}\tag{4.17}$$

where again all of the  $\phi_i^n$  are to be evaluated at  $\frac{1}{4}(2\hat{s} - M^2)$ , and  $\varphi_{\hat{t}}$ ,  $\tilde{\varphi}_{\hat{t}}$  are obtained by replacing  $\hat{s}$  with  $\hat{t}$ . Although the asymptotic behaviour (4.14) is unchanged, in the infrared we now find that, since  $\Sigma(\hat{s})$  is finite for small  $\hat{s}$ ,  $\varphi_{\hat{s}}$  falls to zero linearly with  $\hat{s}$ . This is, as we show explicitly below, just sufficient to cure the infrared divergence by suppressing the emission of Goldstone bosons in the chiral limit. To incorporate this behaviour, we take the new ansätze

$$\varphi_{\hat{s}} = \frac{\hat{s}}{\hat{s} + m_d^2} \varphi\left(\frac{1}{4}(2\hat{s} - M^2)\right), \quad \varphi_{\hat{t}} = \frac{\hat{t}}{\hat{t} - m_d^2} \varphi\left(\frac{1}{4}(M^2 - 2\hat{t})\right),\tag{4.18}$$

with  $\varphi(p^2)$  given by (4.15), and  $\tilde{\varphi}_{\hat{s}}$ ,  $\tilde{\varphi}_{\hat{t}}$  as before.

On the other hand, consistency with the partonic interpretation requires that quarks are treated as massless or quasi-massless. Hence, the present approach will only be justified if the pion mass is sufficiently small that the effects of chiral symmetry breaking in the pseudoscalar meson sector are felt, but also sufficiently large that the inclusion of the quark self energy in the cross-section is not quantitatively important. This will have to be checked explicitly below.

## 5. Computing the Evolution of the Gottfried Sum

The  $Q^2$  dependence of the Gottfried sum is obtained by integrating the meson emission cross-section, eqn.(4.11), over  $\cos\theta$ , taking the first moment, and then using the result to evaluate the evolution factor (3.14). The full analytic expression for the integrated cross-section with the form factors (4.15) is given in the appendix. Even though the general analytic form eqn.(A.1) of the integrated cross section is rather cumbersome, we may understand the main qualitative features of the first moment by considering various limits of it.

In the large- $Q$  limit the first moment of the cross section for any finite  $M$  behaves as

$$\sigma_1^{\gamma^*\Pi}(Q^2)_{Q^2 \rightarrow \infty} \sim \frac{m_d^2(m_d^2 + \Lambda^2)^2}{\pi^2 f_\pi^2} \left[ k_0 + \frac{k_1}{Q^2} + O\left(\frac{1}{Q^4}\right) \right], \quad (5.1)$$

where  $k_0$  and  $k_1$  are dimensionless functions of  $M$ ,  $m_d$ ,  $g_\pi$ ,  $\Lambda$  and  $\tilde{\Lambda}$ . We thus have power suppression of the anomalous dimension at large  $Q^2$ , i.e., “higher-twist” behaviour. This is of course a direct consequence of the presence of the vertex functions  $\phi_i(k, p)$  eqn.(4.4) in the quark–meson coupling (4.2), which forces a deviation from the pointlike behaviour of the emission vertex at large  $Q^2$ . The  $1/Q^2$  falloff is a direct consequence of the soft asymptotic behaviour (4.6); if we had included the logarithms in the ansätze (4.15), we would also have found logarithmic corrections to the higher-twist behaviour. Notice that the anomalous dimension of the Gottfried sum vanishes more rapidly at large  $Q$  than each of the anomalous dimensions for  $\eta$  and  $\pi$  emission does, because the former is proportional to the difference of the latter two.

Furthermore, it is easy to see that the behaviour of the first moment in the large and small meson mass limits at fixed  $Q^2$  is widely different. Indeed, as the meson mass  $M$  tends to zero (the chiral limit) the splitting function reduces to that for the emission of a pointlike pseudoscalar particle, namely (cf eqn.(A.5))

$$\sigma_1^{\gamma^*\Pi}(Q^2)_{M^2 \rightarrow 0} \sim \frac{1}{32\pi^2} \frac{m_d^2(m_d^2 + \Lambda^2)^2}{\Lambda^4 f_\pi^2} \log\left(\frac{Q^2}{M^2}\right). \quad (5.2)$$

This would lead to singular behaviour in the chiral limit due to the usual collinear divergence when the quark propagator in the diagrams of fig. 3 goes on-shell. When the meson mass tends to zero, however, we can no longer neglect the quark self energy, which, due to eqn.(4.18) regulates this divergence in the infrared. We discuss the chiral limit in more detail below; here we merely remark that eqn.(5.2) shows that when the emitted meson is very light the anomalous dimension obtained from eqn.(3.12) is constant, and the scale dependence of all moments is strong.

In the opposite limit of very large meson mass the first moment of the cross section vanishes as

$$\begin{aligned} \sigma_1^{\gamma^*\Pi}(Q^2)_{M \rightarrow \infty} \sim & \frac{2g_\pi^2(m_d^2 + \tilde{\Lambda}^2)^2}{\pi^2 f_\pi^2} \frac{Q^2}{M^4} \left[ 1 + O\left(\frac{1}{M^2}\right) \right] \\ & + \frac{m_d^2(m_d^2 + \Lambda^2)^2}{f_\pi^2} \frac{Q^2}{M^6} \left( \ln\left(\frac{M^2}{Q^2}\right) + c_2 \right) \left[ c_1 + O\left(\frac{1}{M^2}\right) \right], \end{aligned} \quad (5.3)$$



where  $c_1$  and  $c_2$  are dimensionless functions of  $Q^2$ ,  $m_d$ ,  $g_\pi$ ,  $\Lambda$  and  $\tilde{\Lambda}$ . Heavy mesons thus make only a very small contribution to the evolution, as expected. The fall-off of moments of the cross-section at large  $M$  is so rapid because although the cross-section itself only falls as  $1/M^2$ ,  $x_{\max} \sim Q^2/M^2$ . It is interesting to notice that the leading contribution is proportional to  $g_\pi^2$ , because the large  $M$  expansion of the cross-section begins at order  $x$  when  $g_\pi = 0$  (see eqn.(A.6)).

Summarizing, an analysis of various limits of the anomalous dimension computed from the cross section for meson emission confirms the naive expectations discussed in the end of section 2: due to the soft vertex functions, at large  $Q^2$  (compared to all other scales, including  $M$ ) the anomalous dimension always reduces to higher-twist behaviour; for small meson mass (compared to all the other scales, and in particular  $Q^2$ ) the first moment evolves strongly, while for large mass the anomalous dimension is very small, implying that the nonsinglet anomalous dimensions eqn.(3.13), and in particular the combination which governs the evolution of  $S_G$ , are rather large.

We proceed now to a detailed computation of the evolution of the Gottfried sum. In order to do this, we must still fix the free parameters in the cross section eqn.(4.11). As we have seen in the previous section,  $m_d$  may be determined as a function of  $\Lambda$  by the normalization condition eqn.(4.8), or the expression (4.9), with the left hand side determined experimentally to be  $0.38 \pm 0.05 \text{ GeV}^2$ [37]. The resulting dependence of  $m_d$  on  $\Lambda$  is shown in fig. 4, and turns out to be rather weak over a reasonable range of  $\Lambda$ ; moreover, the two independent determinations eqn.(4.8) and (4.9) are compatible within the given uncertainties. In what follows we use for definiteness the value of  $m_d$  determined as a function of  $\Lambda$  by eqn.(4.8), which (see fig. 4) provides us with a lower bound on the anomalous dimension and therefore a conservative estimate of the evolution of the Gottfried sum.  $\Lambda$  is then treated as a free parameter; if  $m_d$  is to be of the order of the constituent quark mass ( $m_d \approx \frac{1}{2}M_\rho \approx \frac{1}{3}M_p$ ),  $\Lambda$  must be roughly in the range  $0.4 \lesssim \Lambda \lesssim 0.8 \text{ GeV}$ .

We are thus left with the parameter  $g_\pi$ , which gives the relative importance of the derivative coupling to the pseudoscalar coupling of the meson to the quark, eqn.(4.2). The sign of  $g_\pi$  is irrelevant, as is apparent from eqn.(4.11). Solutions of truncated Bethe-Salpeter equations seem to indicate that  $\phi_1$  and  $\phi_2$  are rather small[36], but fall off on the same scale as  $\phi_0$ ; according to (4.12) and (4.15) this suggests  $g_\pi < 1$  and  $\tilde{\Lambda} \simeq \Lambda$ . However if quark self energy corrections are included, then  $\phi_0$  also contributes to  $\tilde{\varphi}$  ((4.17)), suggesting

that  $g_\pi \sim 1$ <sup>10</sup>. We thus consider  $0 \leq g_\pi \leq 1$  to be a realistic range of values, and take  $\tilde{\Lambda} = \Lambda$ . This choice is actually immaterial for small values of  $Q^2$ , up to  $Q^2$  of order of a few  $\text{GeV}^2$ , since the contribution of the terms proportional to  $g_\pi$  is negligible in this region. This is due to the fact that terms proportional to  $g_\pi$  yield a negligible contribution to the cross section in most of phase space, and in particular vanish in the region where the form factors are pointlike (and, more generally, whenever their arguments are equal). However they have a slower fall-off at large  $Q^2$  than the rest of the cross-section (because the piece of  $K_1$  (eqn.(A.4)) which is proportional to  $g_\pi^2$  grows as  $\ln Q^2$ ) and thus dominate it asymptotically.

We have thus computed numerically the first moment of the integrated cross-section eqn.(A.1) for  $\pi^0$ ,  $\pi^\pm$ ,  $\eta$  and  $\eta'$  emission, and the derivatives of these first moments with respect to  $\ln Q^2$ , which give the anomalous dimension for nonsinglet evolution according to eqn.(3.8). The results are displayed in fig. 5 (cross section) and fig. 6 (anomalous dimension), where the dependence on the meson mass and on the parameter  $\Lambda$  (with  $g_\pi = 1$ ) are also shown. It is apparent that the contribution to the anomalous dimension from  $\pi$  emission is indeed significantly larger than that from  $\eta$  emission, thereby leading to substantial evolution of the first moment for values of  $Q^2$  between 0.1 and 100  $\text{GeV}^2$ . At small  $Q^2$  the cross-sections evolve very slowly; furthermore, their derivatives tend to a common value, thereby leading to vanishing of the anomalous dimension and flattening of the nonsinglet evolution. For large  $Q^2$  the cross section flattens; the precise value where this occurs is controlled by the parameter  $g_\pi$  and may vary from  $Q^2 \sim 10 \text{ GeV}^2$  for  $g_\pi = 0$  to  $Q^2 \sim 10^3 \text{ GeV}^2$  for  $g_\pi = 1$ .

The relative importance of various contributions to the cross section in different  $Q^2$  regions, as well as the dependence on  $g_\pi$  are displayed in fig. 7. It appears that  $t$ -channel pseudoscalar emission (fig. 3b) provides the leading contribution in the very small  $Q^2 \sim 0.01\text{--}0.1 \text{ GeV}^2$  region;  $s$ -channel emission (fig. 3a) provides the dominant contribution in the small to intermediate  $Q^2 \sim 0.1\text{--}1 \text{ GeV}^2$  region; and the derivative coupling terms, proportional to  $g_\pi$ , control the large  $Q^2$  tail. Comparing fig. 7a ( $\pi^0$  emission) with fig. 7b ( $\eta'$  emission) demonstrates explicitly the relatively slower fall-off (5.3) of the derivative coupling terms compared to the nonderivative ones with increasing meson mass  $M$ .

The  $x$ -dependence of the  $s$  and  $t$  channel contributions which, upon integration, lead to the total cross section of fig. 7a is further displayed in fig. 8. This shows that indeed

---

<sup>10</sup> Although these contributions are either soft, or suppressed by  $\bar{m}/m_d$ , where  $\bar{m}$  is the light current quark mass.

the nonperturbative evolution is dominated by the collinear region where the leading logarithmic approximation holds and the form factors are almost pointlike. It is interesting to observe that in the  $s$ -channel the collinear region is dominant despite the fact that this is the large- $x$  region, and the cross-section vanishes at  $x = x_{\max}$ .

The flattening of the evolution at small  $Q^2$  identifies naturally a scale at which physical observables should be connected smoothly to the quark-model values, which one expects to hold in the infrared regime. It is pleasing to notice that the flattening occurs at  $Q^2 \sim (200 \text{ MeV})^2$ , the natural “QCD scale” at which confinement and chiral symmetry breaking are expected to occur. Moreover the consistency condition resulting from (3.11) can indeed be satisfied in this region (and in no other); when  $\gamma_1^{qq} \simeq 0$ ,  $\pi_1 \simeq 0$ . At this scale there is no dynamically generated meson component, hence the sea is expected to be symmetric and  $S_G$  take its quark model, valence value  $S_G = \frac{1}{3}$ . This result cannot be compared directly with those obtained in effective models (such as Skyrme or chiral quark soliton models) because in such models there is no scale dependence.

We can thus proceed to compute the scale dependence of the Gottfried sum assuming that it takes the quark model value  $S_G = \frac{1}{3}$  at a reference scale  $Q_0 = 200 \text{ MeV}$ , where the evolution flattens, and then using eqn.(2.7). We take  $\Lambda = \tilde{\Lambda}$  and we let this parameter vary in the range discussed above, while we fix  $m_d$  from fig. 4 (solid line), i.e. from eqn.(4.8); we then vary  $0 \leq g_\pi \leq 1$ . Good agreement with the experimental data is obtained for  $\Lambda \approx 550 \text{ MeV}$ , as shown by fig. 9, where both the dependence on  $\Lambda$  and  $g_\pi$  are shown.

Fig. 9 also displays the flattening of the evolution at both small and large  $Q^2$ . Because of the multiplicative character of the evolution the precise small- $Q^2$  value  $Q_0$  at which the condition  $S_G(Q_0) = \frac{1}{3}$  is enforced is immaterial. Indeed, we have checked explicitly that if instead of taking  $Q_0 = 200 \text{ MeV}$ , we fix  $Q_0$  by requiring that the anomalous dimension be smaller than a threshold value (so that  $Q_0$  may depend on the specific values of the parameters) the results are essentially unchanged. The value at which the evolution flattens at large  $Q^2$  is controlled by  $g_\pi$ , and is generally smaller than the value at which the cross section for the emission of each particle separately flattens, as we discussed above. The flattening occurs thus typically around  $Q^2 \sim 3 \text{ GeV}^2$  in the extreme case of  $g_\pi = 0$ , and  $Q^2 \sim 100 \text{ GeV}^2$  if  $g_\pi = 1$ .

In any case, we predict that there is a significant scale dependence of  $S_G$  in the region of  $Q^2 \sim 1 \text{ GeV}^2$ , which could be experimentally detectable. Furthermore, unless  $g_\pi \ll 1$ , it appears that the asymptotic value of  $S_G$  is not yet attained in the region where present-day data are taken; rather, the asymptotic value can be as low as  $S_G(\infty) \approx 0.20$  if  $g_\pi \sim 1$ .

We can now address the issue of the self-consistency of the present approach. Firstly, the very fact of finding a positive value of the anomalous dimensions is of itself nontrivial; there is no fundamental reason why the cross section for meson emission should always increase with  $Q^2$ . This provides an a posteriori consistency check of the probabilistic interpretation of the splitting functions which we have assumed throughout. Furthermore the flattening of the cross-sections at small  $Q^2$  is another nontrivial consistency check; without it we could not assume that the meson component of the sea is generated entirely by  $Q^2$  evolution, due to the condition (3.11). The flattening at large  $Q^2$  is consistent with the asymptotic recovery of perturbative behaviour. A study of the  $x$  and  $Q^2$  dependence of various contributions to the cross-section (figs 7 and 8) shows that indeed significant  $Q^2$  dependence is generated nonperturbatively only when the  $t$ -channel (at small  $Q^2$ ) and the  $s$ -channel evolution (at intermediate  $Q^2$ ) are dominated by the respective quasi-collinear singularities; this is consistent with the probabilistic interpretation of the evolution equations.

Finally, let us consider the chiral limit of our approach. In this limit the cross section eqn.(4.11) diverges in the infrared because the collinear singularities are no longer regulated by the meson mass. This would lead to the behaviour eqn.(5.2) of the splitting function, and thus to an anomalous dimension which does not display higher-twist behaviour at large  $Q^2$ , but rather coincides with that obtained in a theory with pseudoscalar pointlike gluons. This is untenable both theoretically and phenomenologically, and would seem to suggest that the chiral limit reveals an inconsistency in our approach. However, as discussed at the end of section 4, in order to examine the chiral limit consistently it is necessary to compute the meson emission cross sections and the evolution of the Gottfried sum by using the form eqn.(4.18) for the vertex functions, which corresponds to including the self-energy corrections in the internal quark propagator. The external (parton) quarks are kept massless, so the Mandelstam invariants retain their form eqn.(4.13).

In order to simplify the computation, we have approximated the function  $\varphi_{\hat{s}}$  eqn.(4.18) with the linearly rising function  $\varphi_{\hat{s}} = \frac{m_d^3}{f_\pi \Lambda^2} \frac{\hat{s}}{m^2}$  for small  $\hat{s}$ , and the asymptotic form eqn.(4.15) for large  $\hat{s}$ , joined by demanding continuity. An analogous approximation is taken for  $\varphi_{\hat{t}}$ . The dependence of the cross-section on the pseudoscalar meson mass with and without the inclusion of the self energy correction are displayed in fig. 10. It may be seen that the self energy correction does indeed succeed in taming the infrared divergence, thus giving sensible results in the chiral limit.

However, the physical value of  $M_\pi$  is sufficiently large (and thus in practice far from the chiral limit) that the self energy correction makes little difference to the actual evolution of the Gottfried sum. This is shown in fig. 11, where the evolution of the Gottfried sum with and without self-energy corrections are compared (with different values of  $g_\pi$ ). It is thus apparent that the partonic approach is indeed consistent with the smoothness of the chiral limit, since our results for the non-perturbative evolution of the Gottfried sum are essentially insensitive to the dynamical quark mass generation. It is interesting to observe that the normalization of the cross section does depend on the propagating quark mass, but its derivative does not.

We conclude that our approach provides a fully self-consistent, rather stable, and almost parameter-free determination of the anomalous evolution of the Gottfried sum, which allows us to understand the current experimental data in a natural way, and suggests a further  $Q^2$  dependence of the Gottfried sum which may be observable as and when new data at different values of  $Q^2$  become available.

## 6. Conclusion

In this paper we have presented an extension of the Altarelli-Parisi evolution equation to include bound state emission, and computed the relevant splitting functions in the particular case of pseudoscalar emission, which gives the only significant contributions in the nonsinglet channel, due to the large breaking of  $U(N_f)$  flavor symmetry in the pseudoscalar meson spectrum, and the relatively low mass of the pseudo-Goldstone bosons. Our computational method is based on the probabilistic interpretation of the Altarelli-Parisi equations, and leads to a determination of the non-perturbative scale dependence of nonsinglet quark distributions due to the direct coupling of the quarks to the pseudoscalar bound states. We have then determined explicitly the relevant splitting function, we have computed its first moment, and we have determined the scale dependence of the first moment of the nonsinglet quark distribution, and hence that of the Gottfried sum.

The overall qualitative features of our results for the splitting functions and for the evolution of the first moment confirm a posteriori the consistency of our approach: the anomalous dimensions are positive definite (consistently with the probabilistic interpretation), and flatten both at large  $Q^2$ , where they reduce to higher-twist behaviour, and at small  $Q^2$ , around the confinement scale. The evolution of the Gottfried sum is computed

in terms of a single free parameter, which is however fixed independently to within a factor of two, and turns out to be exactly such as needed to explain the recent experimental results, in that it joins smoothly to the quark model value at the confinement scale, and reproduces the observed, significantly smaller value at  $Q^2 = 4 \text{ GeV}^2$ . The evolution has a consistent chiral limit, and is stable upon variation of the parameters.

We believe that the results presented here provide an appealing and consistent resolution of the puzzle posed by the recent data on the Gottfried sum; the value of the sum which is measured experimentally is significantly smaller than the quark model expectation because non-perturbative effects lead to significant evolution in the intermediate  $Q^2$  region. This evolution produces a flavor asymmetry in the quark sea which screens the value of the valence asymmetry, hence the value of the Gottfried sum. The ultimate dynamical reason for this screening is the breaking of the  $U(N_f)$  flavor symmetry to  $SU(N_f)$  in the pseudoscalar meson spectrum due to the chiral anomaly. In this sense, the evolution of the Gottfried sum is anomalous, just as the evolution of the first moment of the polarized structure function  $g_1^p$  [21] is expected to be [24]. Our results also provide a definite, experimentally testable prediction for the scale dependence of the Gottfried sum, and in particular suggest that the asymptotic value of the Gottfried sum may be significantly smaller than the present experimental determination.

Beyond the immediate application to the Gottfried sum, our results provide a rather more general technique for the study of the non-perturbative aspects of deep-inelastic scattering. In particular, it will be interesting to compute the evolution of the full nonsinglet quark densities (not just their first moments) which, at scales below a few GeV, should be rather different from what expected on the basis of perturbative QCD alone. Indeed, there are now experimental indications that the ratio of structure functions  $F_2^n/F_2^p$  evolves differently (i.e. significantly more strongly) than expected perturbatively[38]. Also, the present approach could shed new light on the old idea[39] that the sea distributions are generated radiatively from simple valence distributions at low scales where a quark model valence picture of the nucleon is presumably valid. Whereas all previous attempts to this were hampered by the obvious limitations of perturbative evolution, the present approach could provide the required nonperturbative information. In particular, it is encouraging to note that in contrast to the perturbative evolution the flatness of the non-perturbative evolution at low scales will greatly reduce the sensitivity of the final distributions to the (a priori unknown) starting scale.

The possibility of determining in this way the small- $x$  behaviour of the nonsinglet distributions seems especially intriguing. In the singlet channel, however, the bulk of the evolution will be controlled by the usual perturbative anomalous dimensions, since the nonperturbative anomalous evolution we determine, albeit unusually large for the nonsinglet channel, is always small compared to the singlet perturbative evolution. Nonetheless the effects which we discuss here may still be important in peculiar kinematical ranges, such as very small  $x$  at intermediate  $Q^2$ .

**Acknowledgements:** SF thanks M. Anselmino, V. Barone, L. Magnea, N. N. Nikolaev and E. Predazzi for discussions. RDB would like to thank the Royal Society for financial support.

## Appendix.

The cross-section  $\sigma^{\gamma^*\Pi}(x; Q^2)$ , obtained by integrating the cross-section eqn.(4.11) over  $\cos \theta$ , is given by

$$\begin{aligned}
\sigma_{qq}^{\gamma^*\Pi}(x; Q^2) = & -\frac{1}{\pi^2} \frac{m_d^2(m_d^2 + \Lambda^2)^2}{f_\pi^2} \left\{ \frac{2Q^2(1-x)}{(M^2 + 4\Lambda^2)^2} \frac{(4Q^2 - (3M^2 - 4\Lambda^2)x)}{(Q^2 - M^2x)[2Q^2 - (M^2 - 4\Lambda^2)x]} \right. \\
& + \frac{x(M^2x - Q^2(1-x))}{Q^2(1-x)^2[2Q^2(1-x) - (M^2 - 4\Lambda^2)x]^2} \\
& + \frac{1}{Q^2(M^2 + 4\Lambda^2)^3 [Q^2(1-x) - M^2x] [2Q^2(1-x) - (M^2 - 4\Lambda^2)x]} \\
& \times \left[ 4C_1(x, Q^2, M^2, \Lambda^2) \ln \left( \frac{(1-x)(Q^2 - M^2x)}{M^2x^2} \right) \right. \\
& \quad \left. - C_2(x, Q^2, M^2, \Lambda^2) \ln \left( \frac{x(M^2(1+x) + 4\Lambda^2(1-x))}{(1-x)(2Q^2 - (M^2 - 4\Lambda^2)x)} \right) \right] \\
& + \frac{g_\pi^2}{m_d^2} \frac{(m_d^2 + \tilde{\Lambda}^2)^2}{(m_d^2 + \Lambda^2)^2} \left[ \frac{x(3M^2 - 8\tilde{\Lambda}^2) - 2(M^2 - 4\tilde{\Lambda}^2)x^2 - (1-x)(5-4x)Q^2}{(1-x)[2Q^2(1-x) - (M^2 - 4\tilde{\Lambda}^2)x]^2} \right. \\
& \quad - \frac{1-x}{[M^2(1+x) + 4\tilde{\Lambda}^2(1-x)]} \\
& \quad + \frac{x(1-x)[3(M^2 - 4\tilde{\Lambda}^2)x - 2(3-x)Q^2]}{2[Q^2(1-x) - M^2x][2Q^2(1-x) - (M^2 - 4\tilde{\Lambda}^2)x]} \\
& \quad \left. \times \ln \left( \frac{x(M^2(1+x) + 4\Lambda^2(1-x))}{(1-x)(2Q^2 - (M^2 - 4\Lambda^2)x)} \right) \right] \Bigg\}, \tag{A.1}
\end{aligned}$$

in terms of the parameters defined in section 2 (4.13),(4.15) and with

$$\begin{aligned}
C_1(x, Q^2, M^2, \Lambda^2) = & -2M^2(M^2 + 4\Lambda^2)^2x^2[M^2x - Q^2(1-x)] \\
& + [M^2 + 4\Lambda^2 + (3M^2 - 4\Lambda^2)x] (1-x)Q^4 [(M^2 - 4\Lambda^2)x - Q^2(1-x)], \\
C_2(x, Q^2, M^2, \Lambda^2) = & 2M^2(M^2 - 4\Lambda^2)(M^2 + 4\Lambda^2)^2x^2 [M^2x - Q^2(1-x)] \\
& - [M^2 + 4\Lambda^2 + (3M^2 - 4\Lambda^2)x] Q^4 [M^2 - 4\Lambda^2 + 2Q^2(1-x)^2]. \tag{A.2}
\end{aligned}$$

In the limit of large  $Q^2$  eqn.(A.1) gives

$$\sigma_{qq}^{\gamma^*\Pi}(x; \ln Q^2) = -\frac{1}{\pi^2} \frac{m_d^2(m_d^2 + \Lambda^2)^2}{f_\pi^2} \left[ K_0 + K_1 \frac{1}{Q^2} \right] + O\left(\frac{1}{Q^4}\right), \tag{A.3}$$



where

$$\begin{aligned}
K_0 &= \frac{4(1-x)}{(M^2 + 4\Lambda^2)^2} - \frac{2[M^2(1+3x) + 4\Lambda^2(1-x)]}{(M^2 + 4\Lambda^2)^3} \ln \left( \frac{M^2(1+x) + 4\Lambda^2(1-x)}{2M^2x} \right) \\
&\quad - \frac{g_\pi^2 (m_d^2 + \tilde{\Lambda}^2)^2}{m_d^2 (m_d^2 + \Lambda^2)^2} \frac{(1-x)}{[M^2(1+x) + 4\tilde{\Lambda}^2(1-x)]} \\
K_1 &= \frac{4M^2}{(M^2 + 4\Lambda^2)^2} + \frac{2M^2x[M^2(1+3x) + 4\Lambda^2(1-x)]}{(1-x)(M^2 + 4\Lambda^2)^3} \ln \left( \frac{M^2(1+x) + 4\Lambda^2(1-x)}{2M^2x^2} \right) \\
&\quad + \frac{g_\pi^2 (m_d^2 + \tilde{\Lambda}^2)^2}{m_d^2 (m_d^2 + \Lambda^2)^2} \left[ \frac{x(5-4x)}{4(1-x)^2} - \frac{x(3-x)}{2(1-x)} \ln \left( \frac{x[M^2(1+x) + 4\Lambda^2(1-x)]}{2Q^2(1-x)} \right) \right].
\end{aligned} \tag{A.4}$$

In the limit of small meson mass  $M$  eqn.(A.1) yields

$$\sigma_{qq}^{\gamma^* \Pi}(x; Q^2) = \frac{1}{16\pi^2} \frac{m_d^2(m_d^2 + \Lambda^2)^2}{f_\pi^2 \Lambda^4} (1-x) \ln \left( \frac{Q^2}{M^2} \right) + O(1), \tag{A.5}$$

while in the limit of large meson mass  $M$  eqn.(A.1) reduces to

$$\begin{aligned}
\sigma_{qq}^{\gamma^* \Pi}(x; Q^2) &= -\frac{1}{\pi^2} \frac{m_d^2(m_d^2 + \Lambda^2)^2}{f_\pi^2 M^2} \left\{ \frac{x}{Q^2(1-x)^2} + \frac{2x}{Q^2} \ln \left( \frac{x^2}{1-x^2} \right) \right. \\
&\quad \left. + \frac{g_\pi^2 (m_d^2 + \tilde{\Lambda}^2)^2}{m_d^2 (m_d^2 + \Lambda^2)^2} \left[ \frac{2+3x(1-x)}{(1-x^2)} - \frac{3(1-x)}{2} \ln \left( \frac{1-x}{1+x} \right) \right] \right\} + O\left(\frac{1}{M^4}\right).
\end{aligned} \tag{A.6}$$

The expressions (A.3) and (A.6), however, are not very useful in practice since, for large  $Q^2$ ,  $x_{\max} = 1 - M^2/Q^2 + O(M^4/Q^4)$  and, for large  $M$ ,  $x_{\max} = Q^2/M^2 + O(Q^4/M^4)$ . To obtain the behaviour of the first moment of (A.1) thus it is not enough to take moments of these equations; rather one must expand consistently in both  $1/Q^2$  and  $x$ , or, respectively,  $1/M^2$  and  $x$ , which leads to rather cumbersome expressions which will not be given here.

## References

- [1] J. Ashman et al., *Phys. Lett.* **B206** (1988) 364; *Nucl. Phys.* **B328** (1990) 1.
- [2] P. Amaudruz et al., *Phys. Rev. Lett.* **66** (1991) 560.
- [3] K. Gottfried, *Phys. Rev. Lett.* **18** (1967) 1174 ;  
see also e.g. F. Close “An Introduction to Quarks and Partons” (Academic, London, 1979) or E. Leader and E. Predazzi “Gauge Theories and the New Physics” (Cambridge University, Cambridge, 1982).
- [4] A. D. Martin, W. J. Stirling and R. G. Roberts, *Phys. Lett.* **B252** (1990) 653;  
S. D. Ellis and W. J. Stirling, *Phys. Lett.* **B256** (1991) 258.
- [5] V. R. Zoller, *Phys. Lett.* **B279** (1992) 145;  
B. Badełek and J. Kwieciński, *Nucl. Phys.* **B370** (1991) 278;  
W. Melnitchouk and A. W. Thomas, *Phys. Rev.* **D47** (1993) 3783.
- [6] G. Altarelli, *Phys. Rep.* **81** (1982) 1.
- [7] B. Badełek et al., *Rev. Mod. Phys.* **64** (1992) 927.
- [8] See e.g. T. Sloan, G. Smadja and R. Voss, *Phys. Rep.* **162** (1988) 45.
- [9] S. Forte, *Phys. Rev.* **D47** (1993) 1842.
- [10] A. D. Martin, W. J. Stirling and R. G. Roberts, *Phys. Rev.* **D47** (1993) 867; *Phys. Lett.* **B306** (1993) 145; Rutherford preprints RAL-93-014 and RAL-93-027(1993);  
J. Botts et al., *Phys. Lett.* **B304** (1993) 159.
- [11] D. A. Ross and C. T. Sachrajda, *Nucl. Phys.* **B149** (1979) 497.
- [12] A. Signal, A. W. Schreiber and A. W. Thomas, *Mod. Phys. Lett.* **A6** (1991) 271.
- [13] R. P. Feynman and R. D. Field, *Phys. Rev.* **D15** (1977) 2590.
- [14] A. W. Thomas, *Nucl. Phys.* **A532** (1991) 177.
- [15] S. Kumano, *Phys. Rev.* **D43** (1991) 59 *Phys. Rev.* **D43** (1991) 3067;  
S. Kumano and J. T. Londergan, *Phys. Rev.* **D44** (1991) 717.
- [16] H. Walliser and G. Holzwarth, *Phys. Lett.* **B302** (1993) 377.
- [17] M. Wakamatsu, *Phys. Rev.* **D44** (1991) R2631; *Phys. Rev.* **D46** (1992) 3762.
- [18] A. W. Schreiber et al., *Phys. Rev.* **D45** (1992) 3069.
- [19] E. J. Eichten, I. Hinchliffe and C. Quigg, *Phys. Rev.* **D45** (1992) 2269.
- [20] H. Georgi and A. Manohar, *Nucl. Phys.* **B234** (1984) 189.
- [21] G. Altarelli, in “The Challenging Questions”, Proc. of the 1989 Erice school, A. Zichichi, ed. (Plenum, New York, 1990) ;  
G. G. Ross in “Proc. of the 1989 Int. Symp. on Lepton and Photon Interactions at High Energy”, Stanford, 1989 (World Scientific, Singapore, 1989) ;  
G. Veneziano in “From Symmetries to Strings”, proc. of the Okubofest, Rochester, 1989, A. Das, ed. (World Scientific, Singapore, 1990) ;  
J. Ellis, *Nucl. Phys.* **A546** (1992) 447c.
- [22] G. 't Hooft, *Phys. Rep.* **142** (1986) 357 and ref. therein.

- [23] S. Forte, *Nucl. Phys.* **B331** (1990) 1;  
S. Forte and E. V. Shuryak, *Nucl. Phys.* **B357** (1991) 153.
- [24] R. D. Ball, *Phys. Lett.* **B266** (1991) 473.
- [25] A. V. Manohar, Lectures at Lake Louise Winter Inst., Canada, 1992, San Diego preprint UCSD/PTH 92-10 (1992).
- [26] L. Durand and W. Putikka, *Phys. Rev.* **D36** (1987) 2840;  
J. C. Collins and J. Qiu, *Phys. Rev.* **D39** (1989) 1398.
- [27] S. J. Chang and P. M. Fishbane, *Phys. Rev.* **D2** (1972) 1084;  
V. N. Gribov and L. N. Lipatov, *Sov. Jour. Nucl. Phys.* **15** (1972) 438, 675;  
see also Y. L. Dokshitzer, D. I. Diakonov and S. I. Troyan, *Phys. Rep.* **58** (1980) 269.
- [28] C. H. Llewellyn Smith, in “Facts and Prospects of Gauge Theories”, proc. of the 1978 Schlading school, P. Urban, ed. (Springer, Wien, 1978).
- [29] J. D. Sullivan, *Phys. Rev.* **D5** (1972) 1732 ;  
A. W. Thomas, *Phys. Lett.* **B126** (1983) 97.
- [30] R. Jackiw and K. Johnson, *Phys. Rev.* **D8** (1973) 2386.
- [31] C. H. Llewellyn Smith *Ann. Phys. (NY)* **53** (1969) 521.
- [32] H. Pagels, *Phys. Rev.* **D15** (1977) 2991; **D19** (1979) 3080; **D21** (1980) 2337.
- [33] H. Pagels and S. Stokar, *Phys. Rev.* **D20** (1979) 2947.
- [34] R. D. Ball, *Int. Jour. Mod. Phys.* **A5** (1990) 4391.
- [35] B. Holdom, *Phys. Rev.* **D45** (1992) 2535;  
R. D. Ball and G. Ripka, in preparation.
- [36] R. D. Ball and J. Tigg, unpublished.
- [37] C. J. Bebek et al., *Phys. Rev.* **D13** (1976) 25; **D17** (1978) 1693.
- [38] P. Amaudruz et al., CERN preprint CERN-PPE/91-167 (1991).
- [39] G. Parisi and R. Petronzio, *Phys. Lett.* **B62** (1976) 331 ;  
V.A. Novikov, M.A. Shifman, A.I. Vainshtein and V.I. Zakharov, *Ann. Phys.* **105** (1977) 276 ;  
M. Glück and E. Reya, *Nucl. Phys.* **B130** (1977) 76.

## Figure Captions

- [Fig. 1] The two-loop diagram which generates nonsinglet evolution of structure functions. When  $i = j$  the final state must be antisymmetrized.
- [Fig. 2] The diagram responsible for flavor symmetry breaking non-perturbative evolution.
- [Fig. 3] Deep-inelastic scattering off a quark which radiates a bound state  $\Pi$ : a)  $t$ -channel diagram; b)  $s$ -channel diagram.
- [Fig. 4] The constituent mass  $m_d$  as a function of  $\Lambda$ , as given by eqn.s (4.8) (full line) and (4.9) (dashed line; the dotted lines correspond to the experimental uncertainty).
- [Fig. 5] First moment  $\sigma_1^{\gamma^*\Pi}$  of the cross-section eqn.(4.11) computed with  $\tilde{\Lambda} = \Lambda$ ,  $g_\pi = 1$  and  $m_d$  fixed from the full line of fig. 4: a)  $\Pi = \pi^0$ ; b)  $\Pi = \eta'$ ; c)  $\Lambda = 600$  MeV.
- [Fig. 6] Anomalous dimensions  $\gamma_1^{qq} = \frac{d}{dt}\sigma_1^{\gamma^*\Pi}$  computed from the cross sections displayed in fig. 5.
- [Fig. 7] Contributions of various terms in eqn.(4.11) to the cross section displayed in fig. 5a with  $\Lambda = 600$  MeV: full line, cross section with  $g_\pi = 0$ ; dot-dash line, cross section with  $g_\pi = \frac{1}{2}$ ; dotted line,  $s$ -channel contribution (obtained setting  $\phi_{\hat{t}} = g_\pi = 0$  in eqn.(4.11)); dashed line,  $t$ -channel contribution (obtained setting  $\phi_{\hat{s}} = g_\pi = 0$  in eqn.(4.11)).
- [Fig. 8] Dependence on  $x$  of the  $s$ -channel and  $t$ -channel contributions whose integral with respect to  $x$  is shown in fig. 7a, with several values of  $Q^2$ : a)  $t$ -channel contributions (dotted lines of fig. 7a); b)  $s$ -channel contributions (dashed lines of fig. 7a).
- [Fig. 9] Scale dependence of the Gottfried sum, computed with  $\tilde{\Lambda} = \Lambda$  and  $m_d$  fixed from the solid curve in fig. 4: a)  $g_\pi = 1$ ; b) solid curves,  $g_\pi = 1$ ; dotted curves,  $g_\pi = \frac{1}{2}$ ; dashed curves,  $g_\pi = 0$ . The experimental value eqn.(1.2) (uncorrected for shadowing) is also displayed.
- [Fig. 10] The approach to the chiral limit of the first moment of the integrated cross section: a) Without self-energy corrections; b) with self-energy corrections. The values of the parameters are the same as in fig. 5c.
- [Fig. 11] Detail of the scale dependence of the Gottfried sum: solid curve, as the solid curve in fig. 9b ( $g_\pi = 1$ ); dotted curve, same with dynamical mass correction; dashed curve, as the dashed curve in fig. 9b ( $g_\pi = 0$ ); dash-dot curve, same with the dynamical mass corrections. The values of the parameters are the same as in the curves of fig. 8 but with  $\Lambda = 500$  MeV.

This figure "fig1-1.png" is available in "png" format from:

<http://arxiv.org/ps/hep-ph/9308322v1>

This figure "fig2-1.png" is available in "png" format from:

<http://arxiv.org/ps/hep-ph/9308322v1>

This figure "fig1-2.png" is available in "png" format from:

<http://arxiv.org/ps/hep-ph/9308322v1>

This figure "fig2-2.png" is available in "png" format from:

<http://arxiv.org/ps/hep-ph/9308322v1>



This figure "fig2-3.png" is available in "png" format from:

<http://arxiv.org/ps/hep-ph/9308322v1>

This figure "fig2-4.png" is available in "png" format from:

<http://arxiv.org/ps/hep-ph/9308322v1>

This figure "fig2-5.png" is available in "png" format from:

<http://arxiv.org/ps/hep-ph/9308322v1>

This figure "fig2-6.png" is available in "png" format from:

<http://arxiv.org/ps/hep-ph/9308322v1>

This figure "fig2-7.png" is available in "png" format from:

<http://arxiv.org/ps/hep-ph/9308322v1>

This figure "fig2-8.png" is available in "png" format from:

<http://arxiv.org/ps/hep-ph/9308322v1>

This figure "fig2-9.png" is available in "png" format from:

<http://arxiv.org/ps/hep-ph/9308322v1>

This figure "fig2-10.png" is available in "png" format from:

<http://arxiv.org/ps/hep-ph/9308322v1>



This figure "fig2-11.png" is available in "png" format from:

<http://arxiv.org/ps/hep-ph/9308322v1>

This figure "fig2-12.png" is available in "png" format from:

<http://arxiv.org/ps/hep-ph/9308322v1>

This figure "fig2-13.png" is available in "png" format from:

<http://arxiv.org/ps/hep-ph/9308322v1>

This figure "fig2-14.png" is available in "png" format from:

<http://arxiv.org/ps/hep-ph/9308322v1>

This figure "fig2-15.png" is available in "png" format from:

<http://arxiv.org/ps/hep-ph/9308322v1>

This figure "fig2-16.png" is available in "png" format from:

<http://arxiv.org/ps/hep-ph/9308322v1>

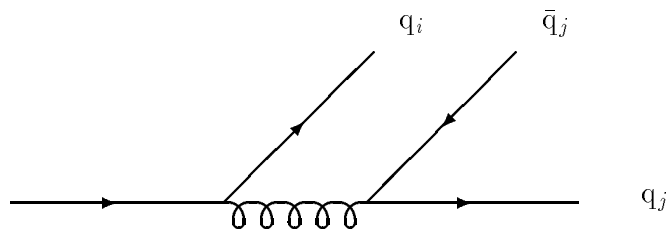


Fig. 1

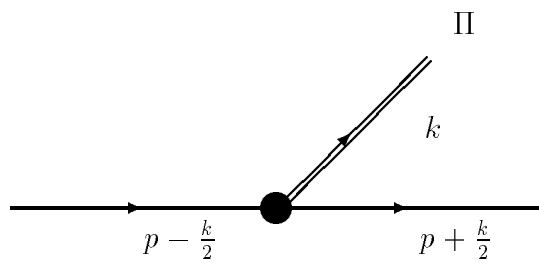


Fig. 2

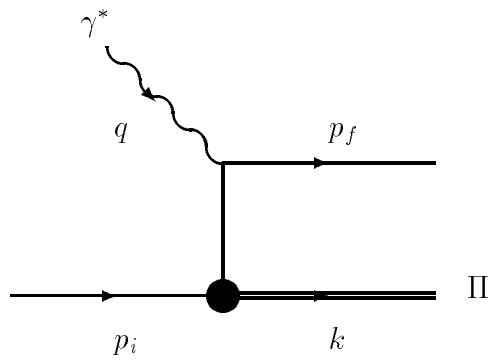


Fig. 3a

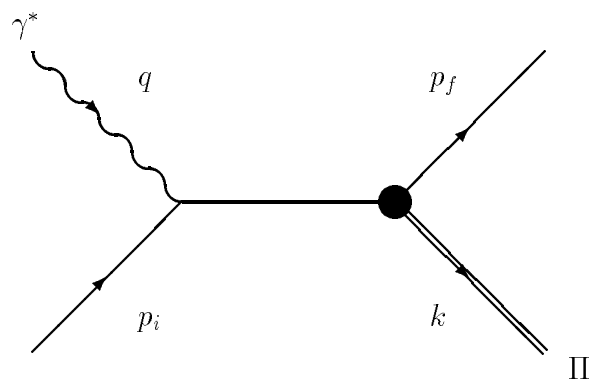


Fig. 3b



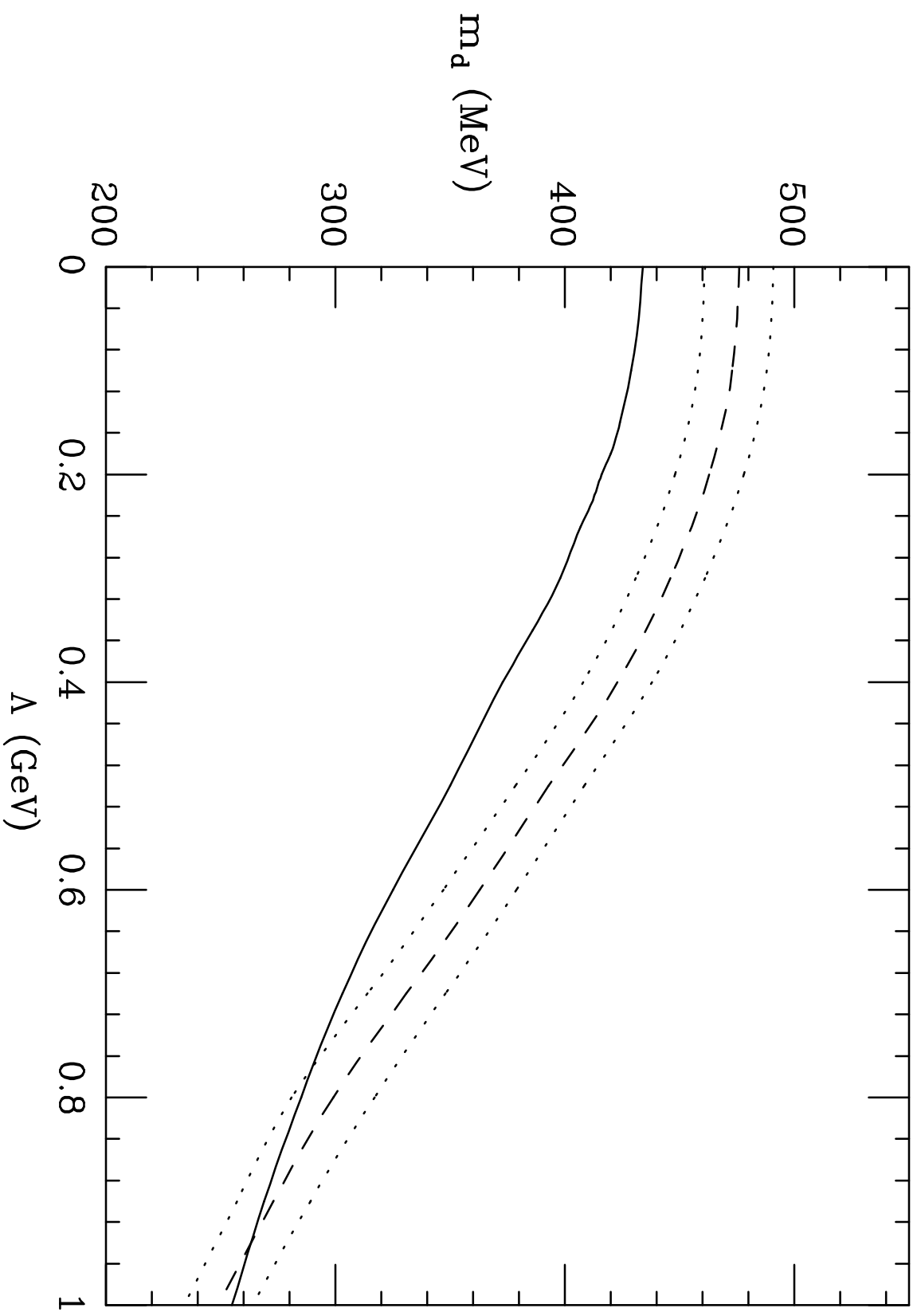


Fig. 4

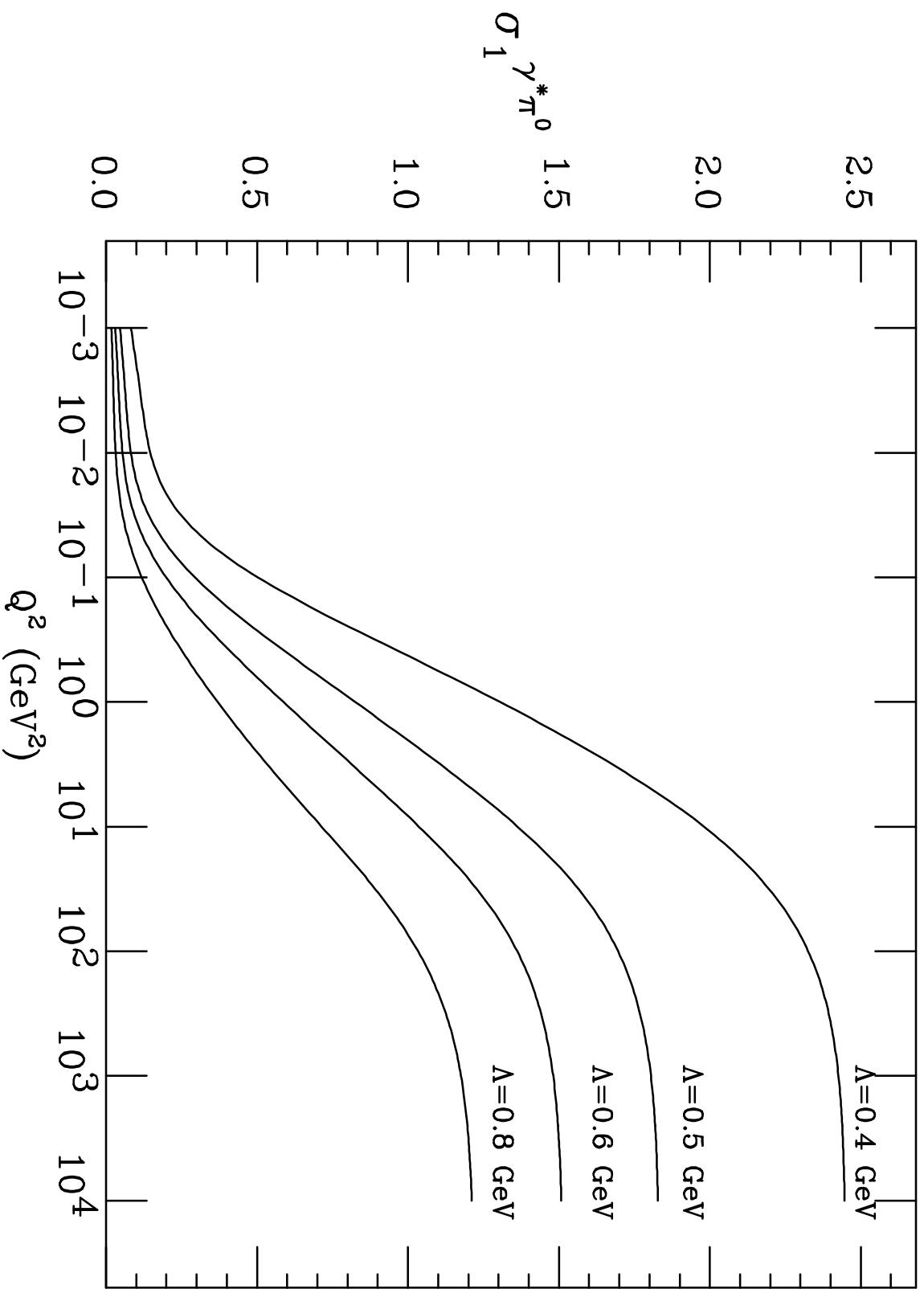


Fig. 5a

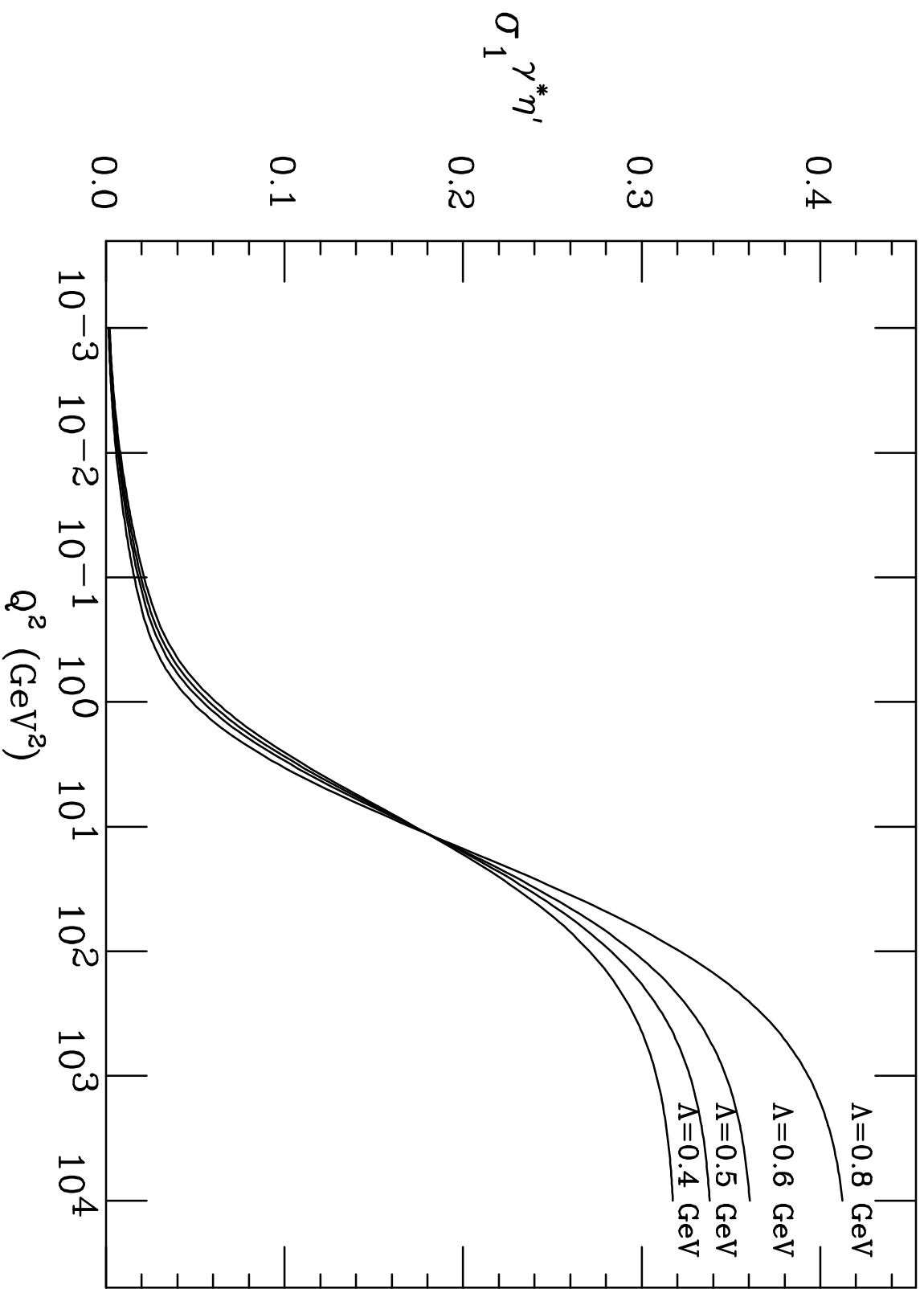


Fig. 5b

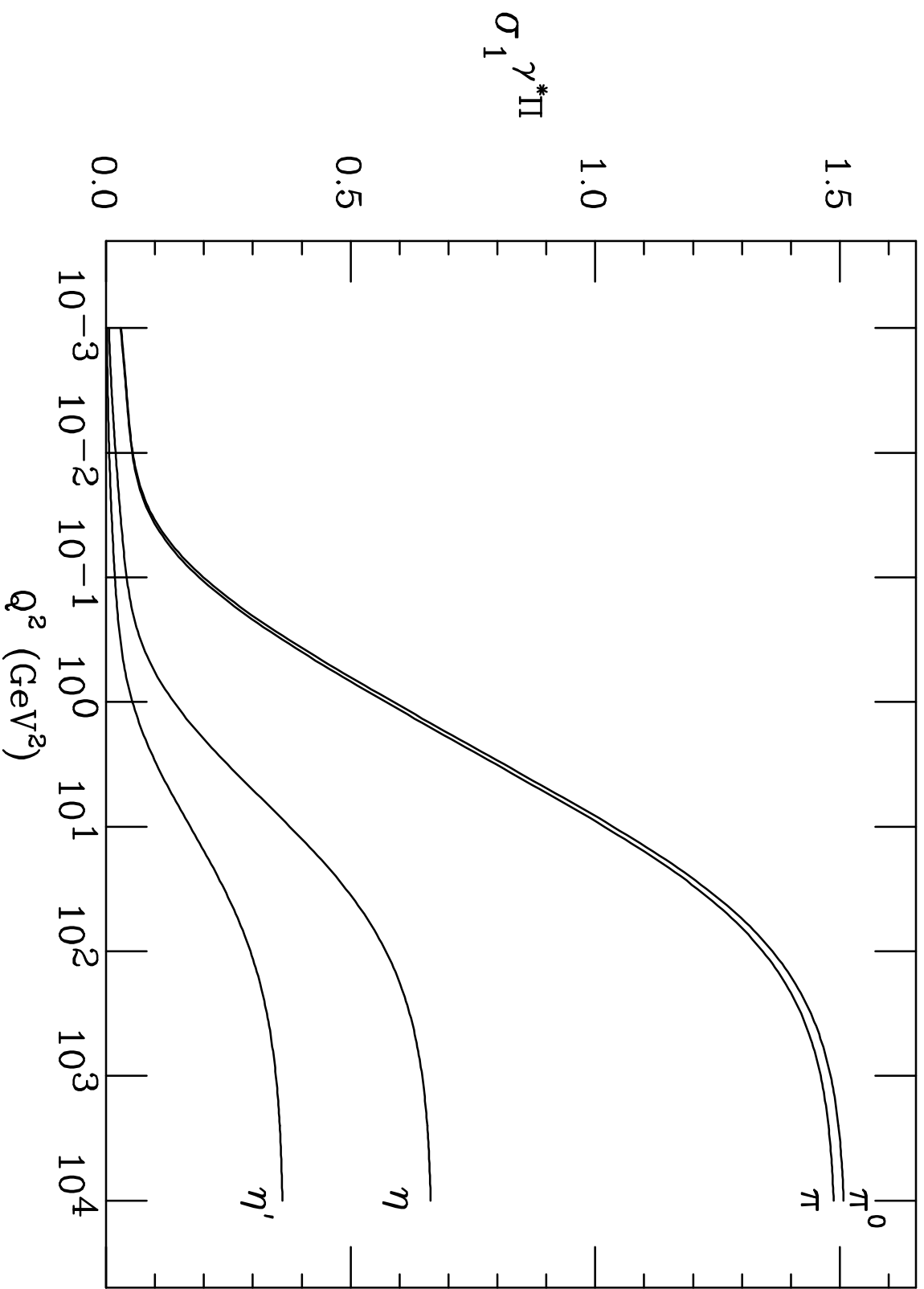


Fig. 5c

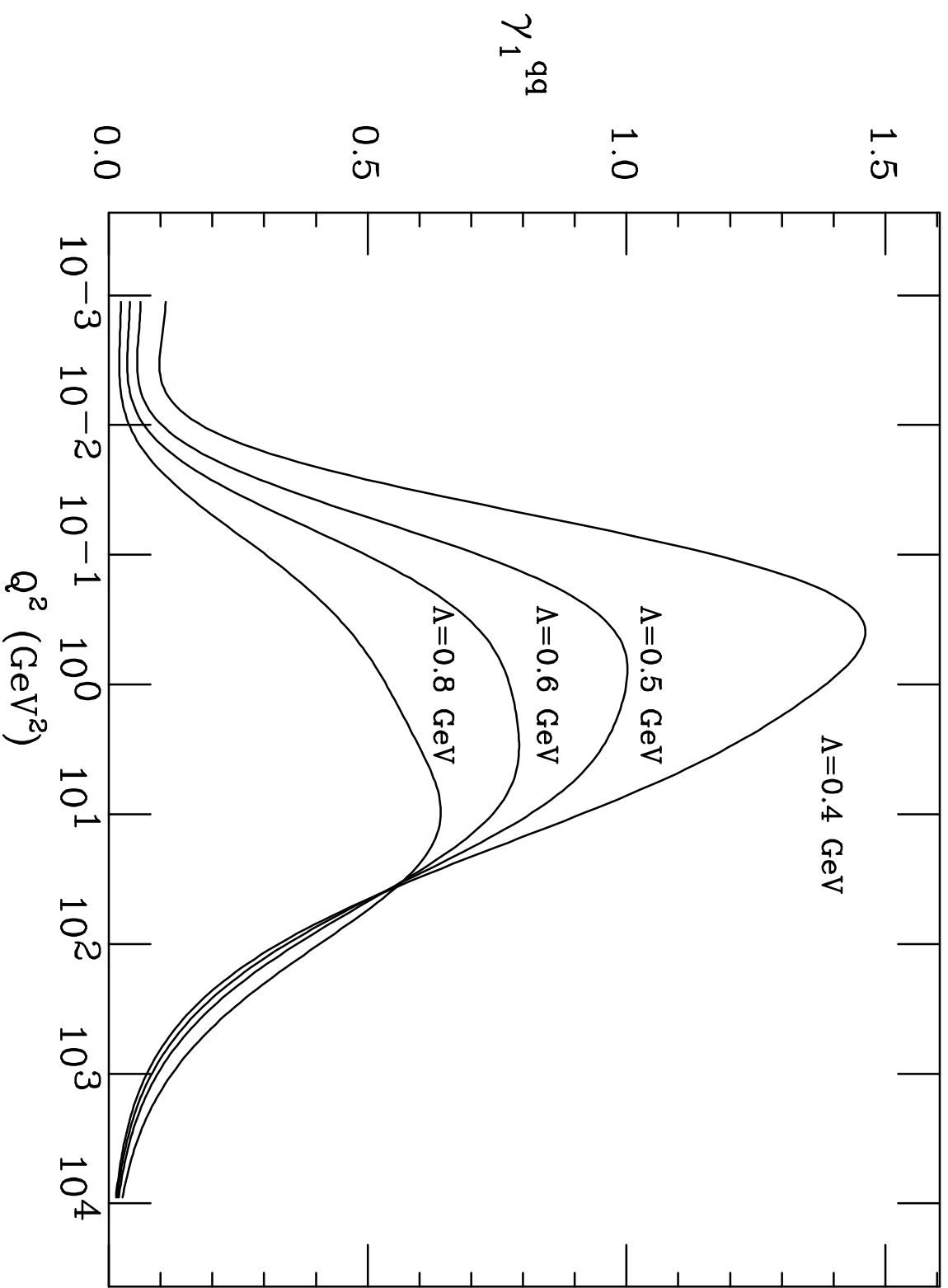


Fig. 6a

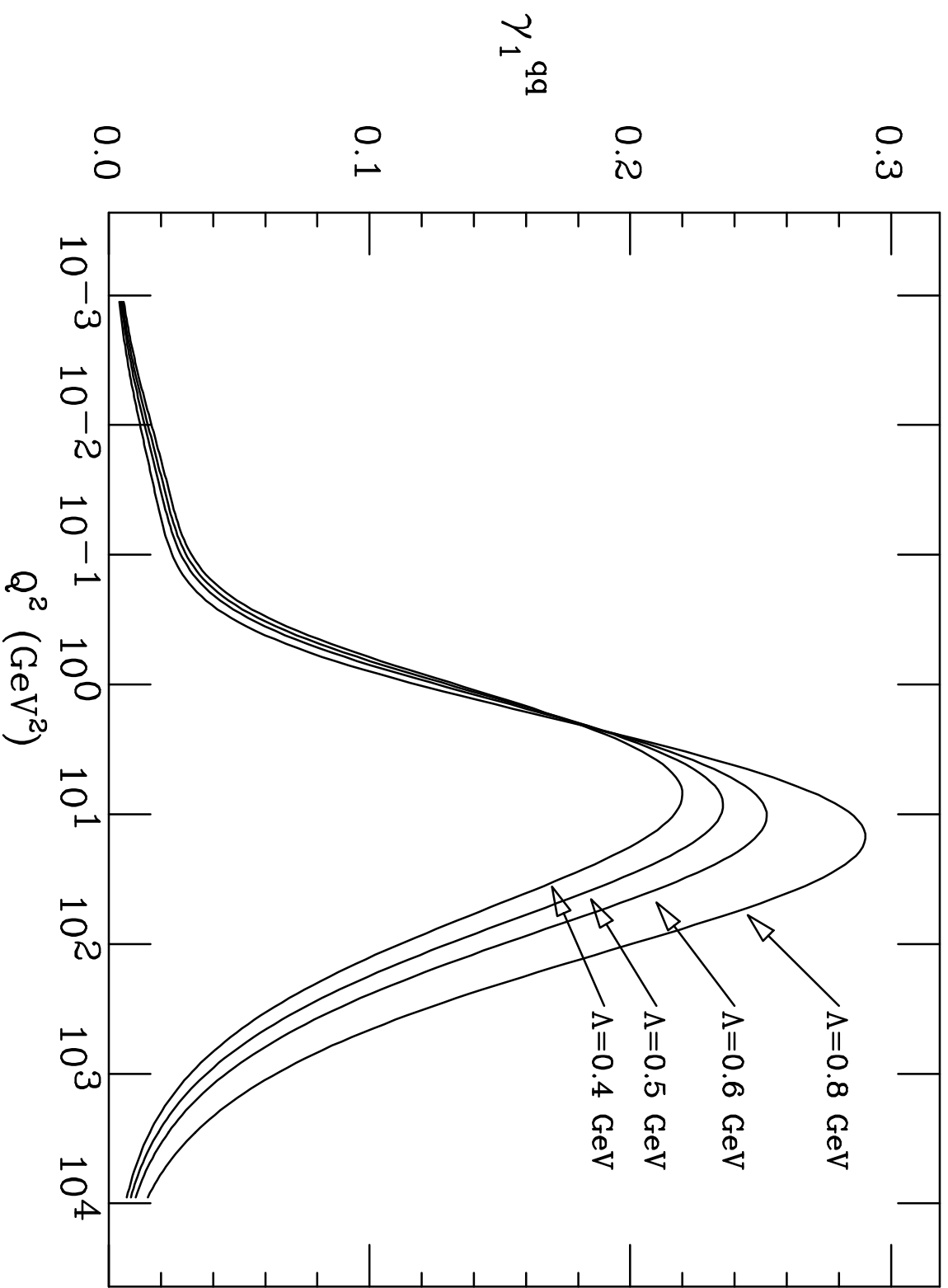


Fig. 6b

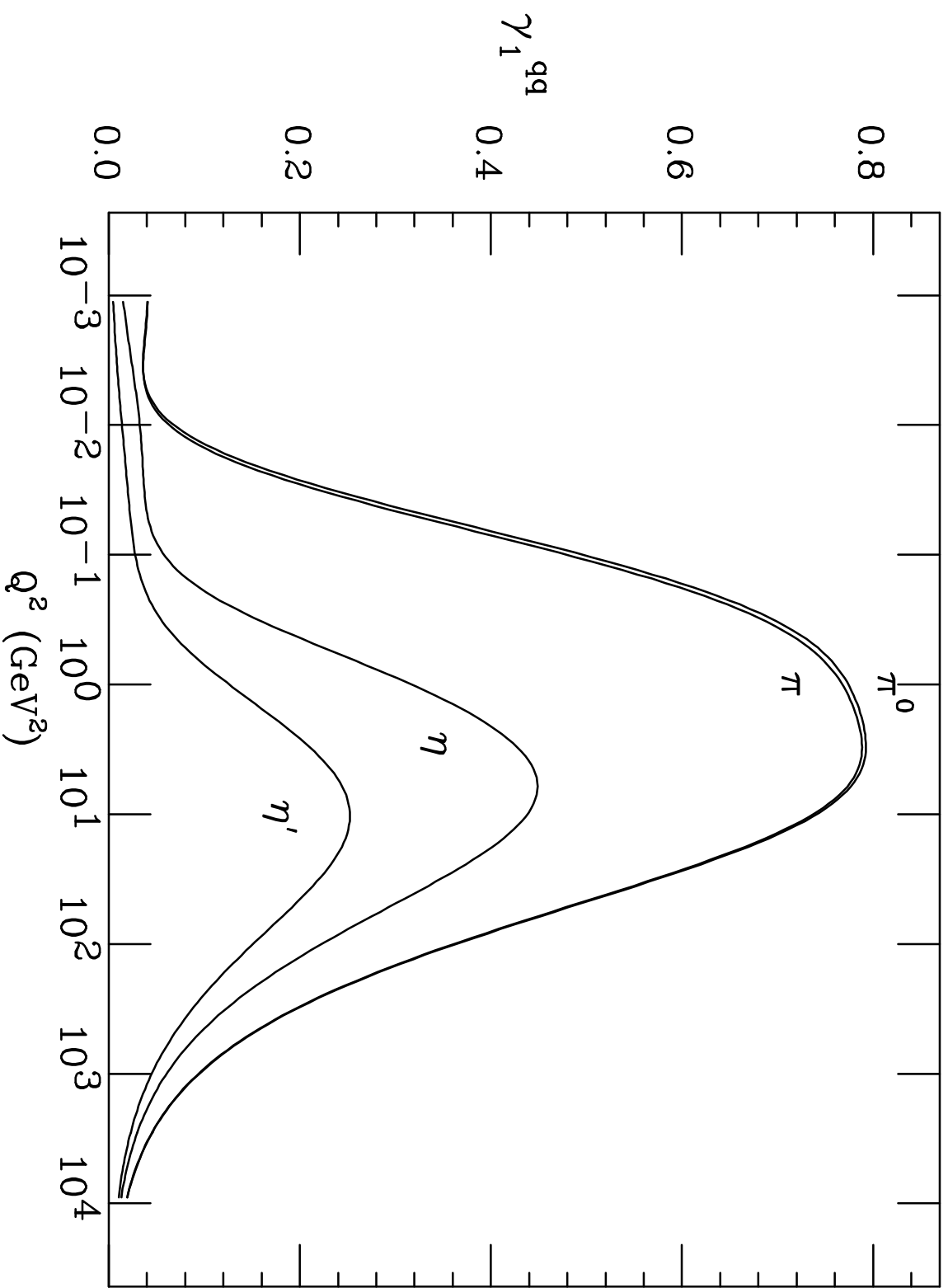


Fig. 6c

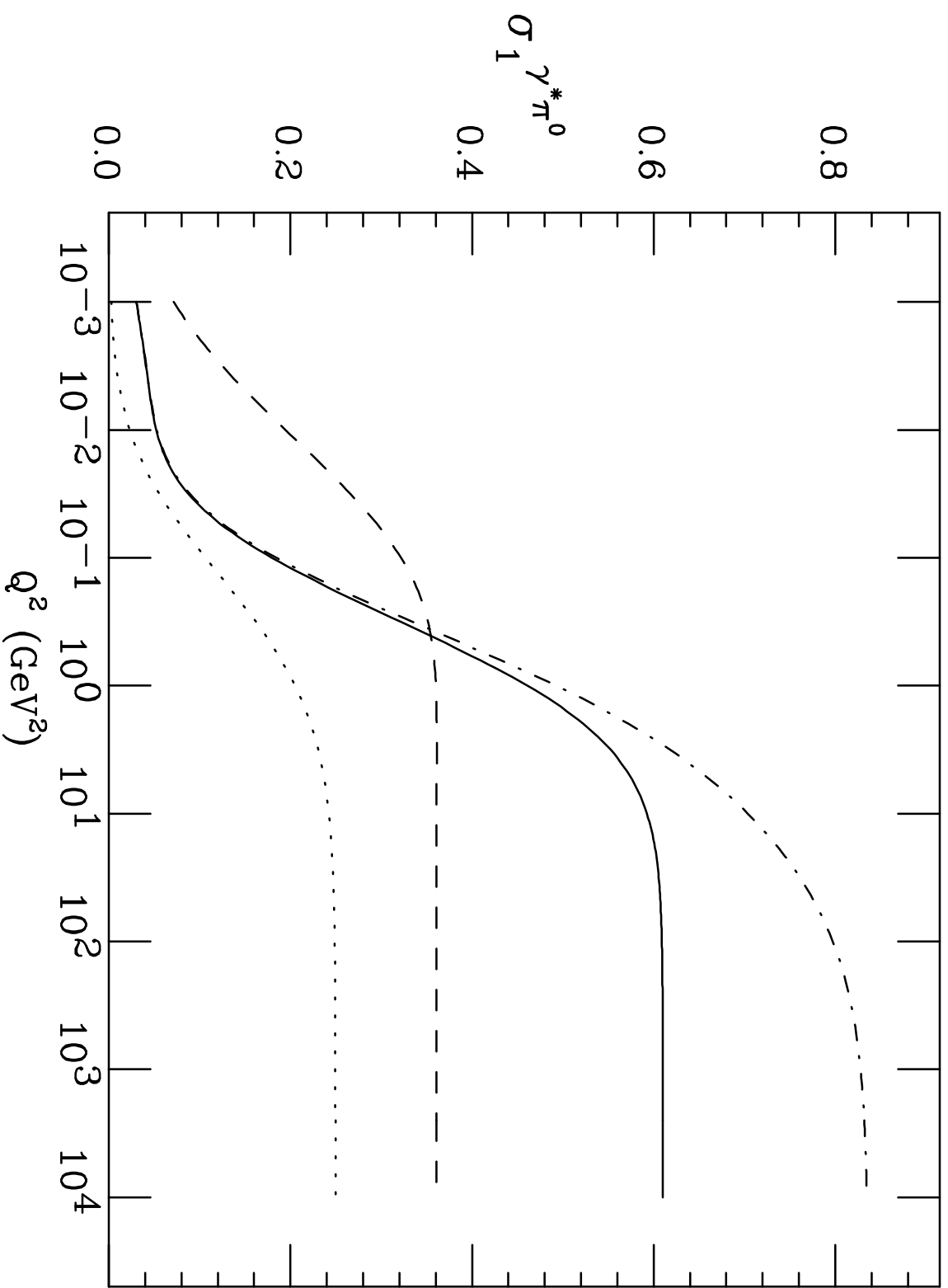


Fig. 7a



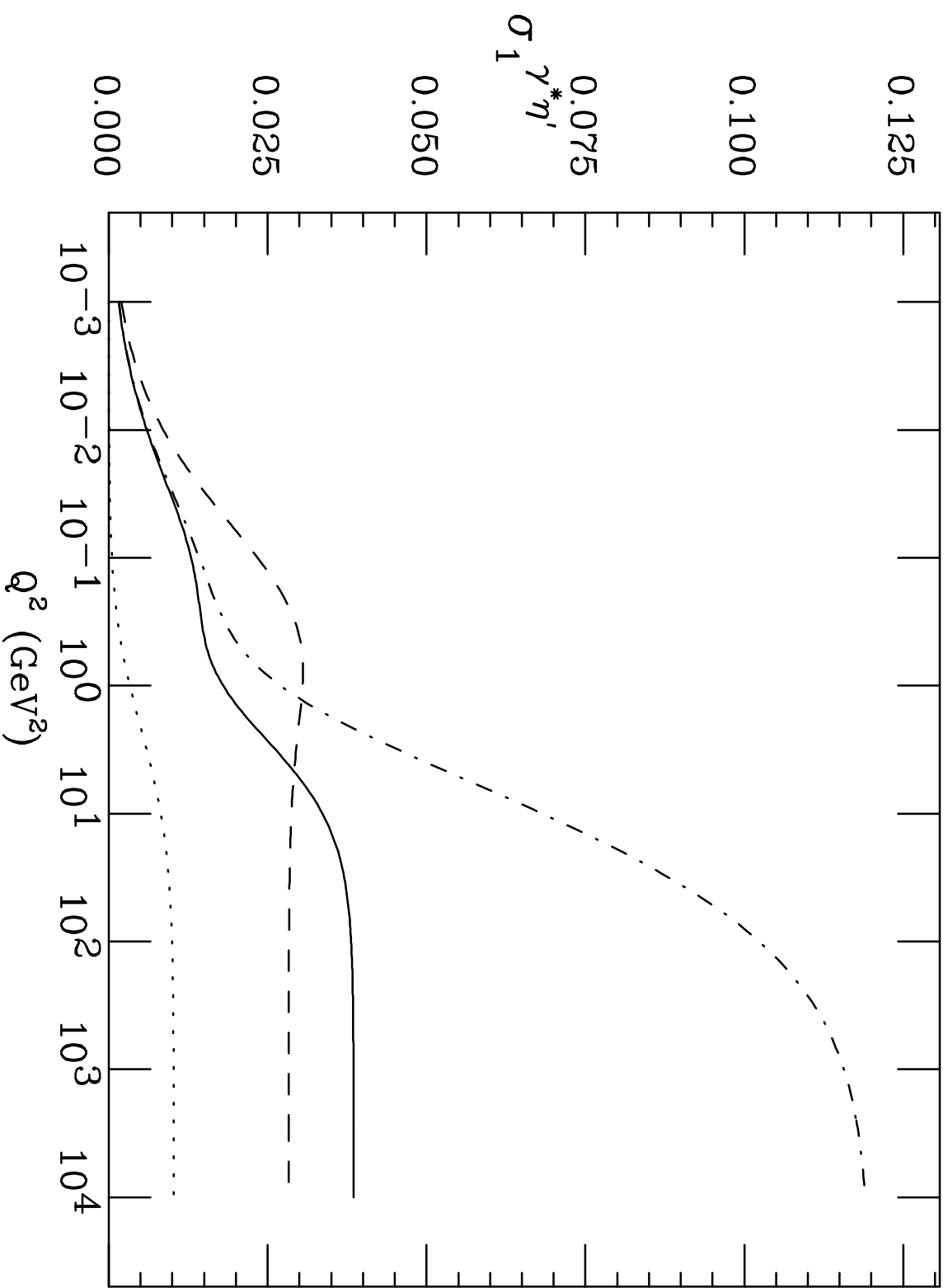


Fig. 7b

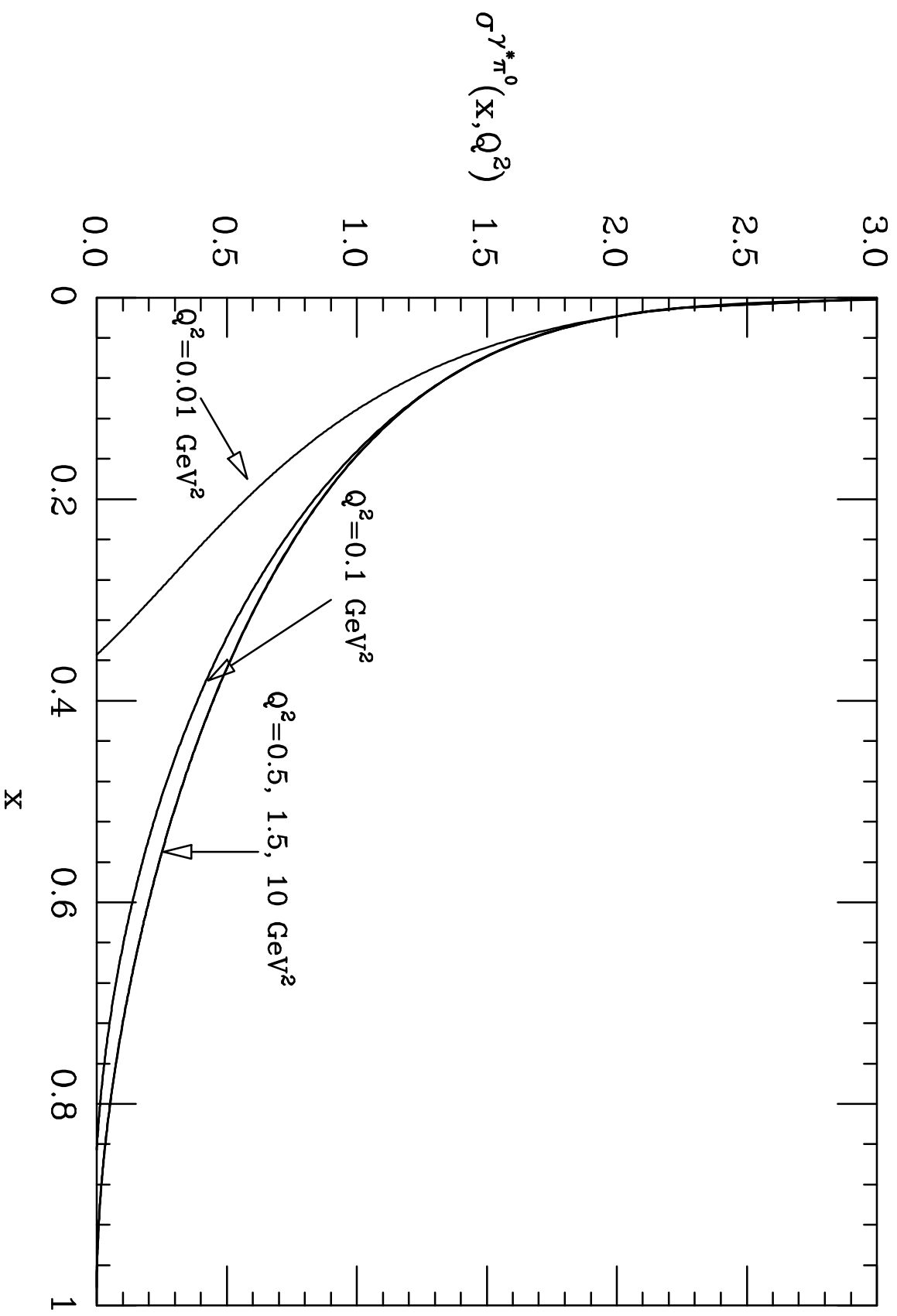


Fig. 8a

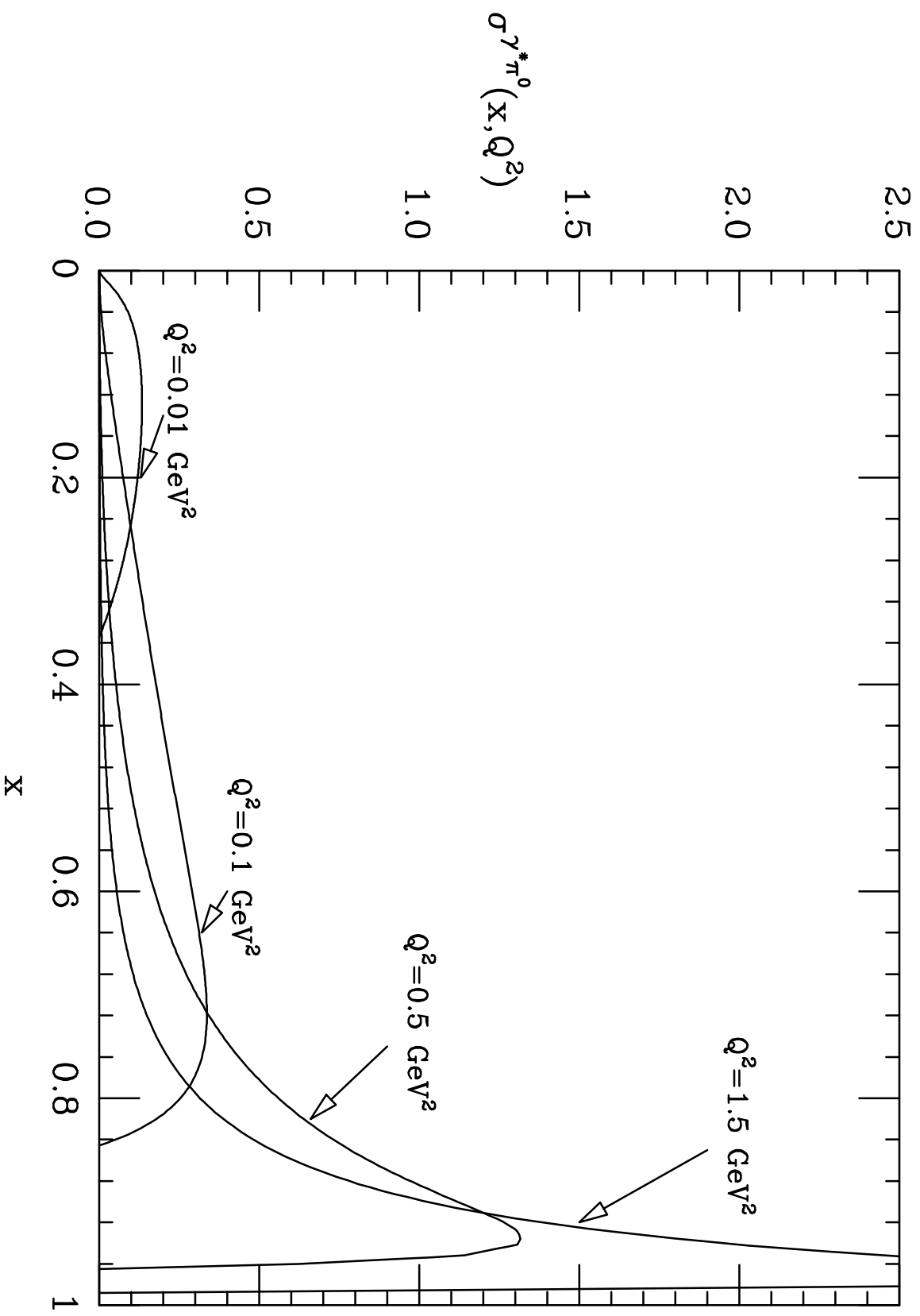


Fig. 8b

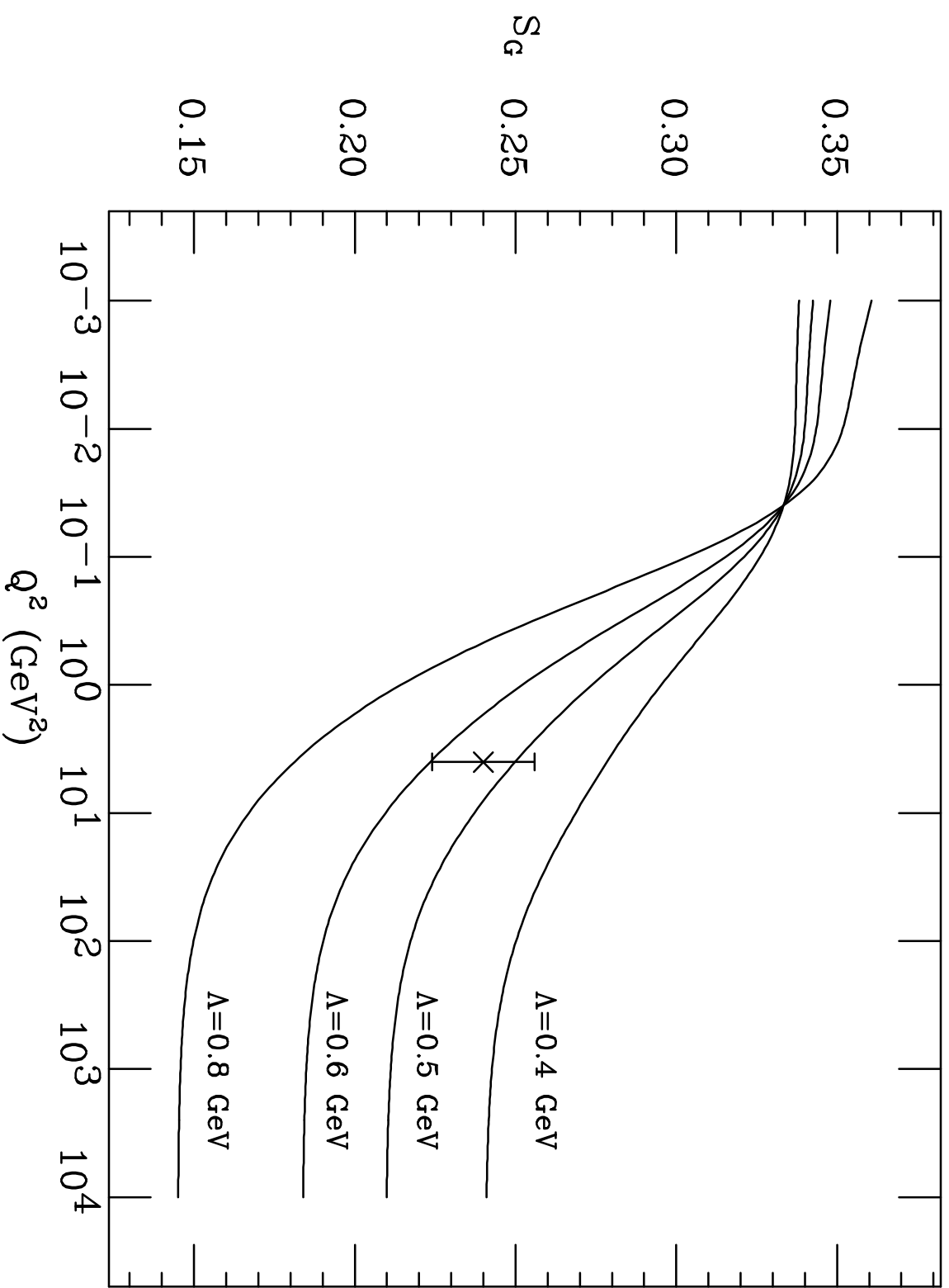


Fig. 9a

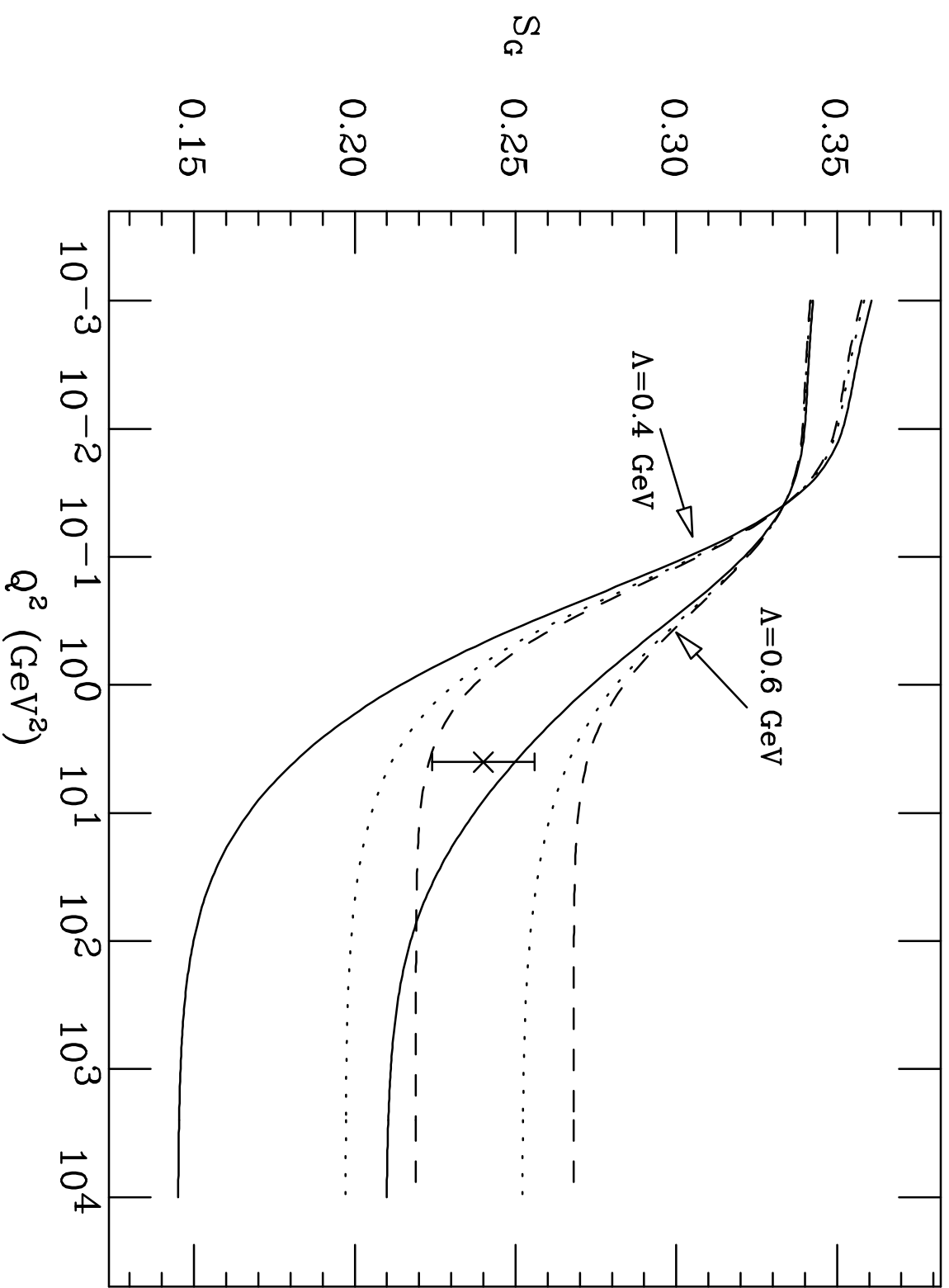


Fig. 9b

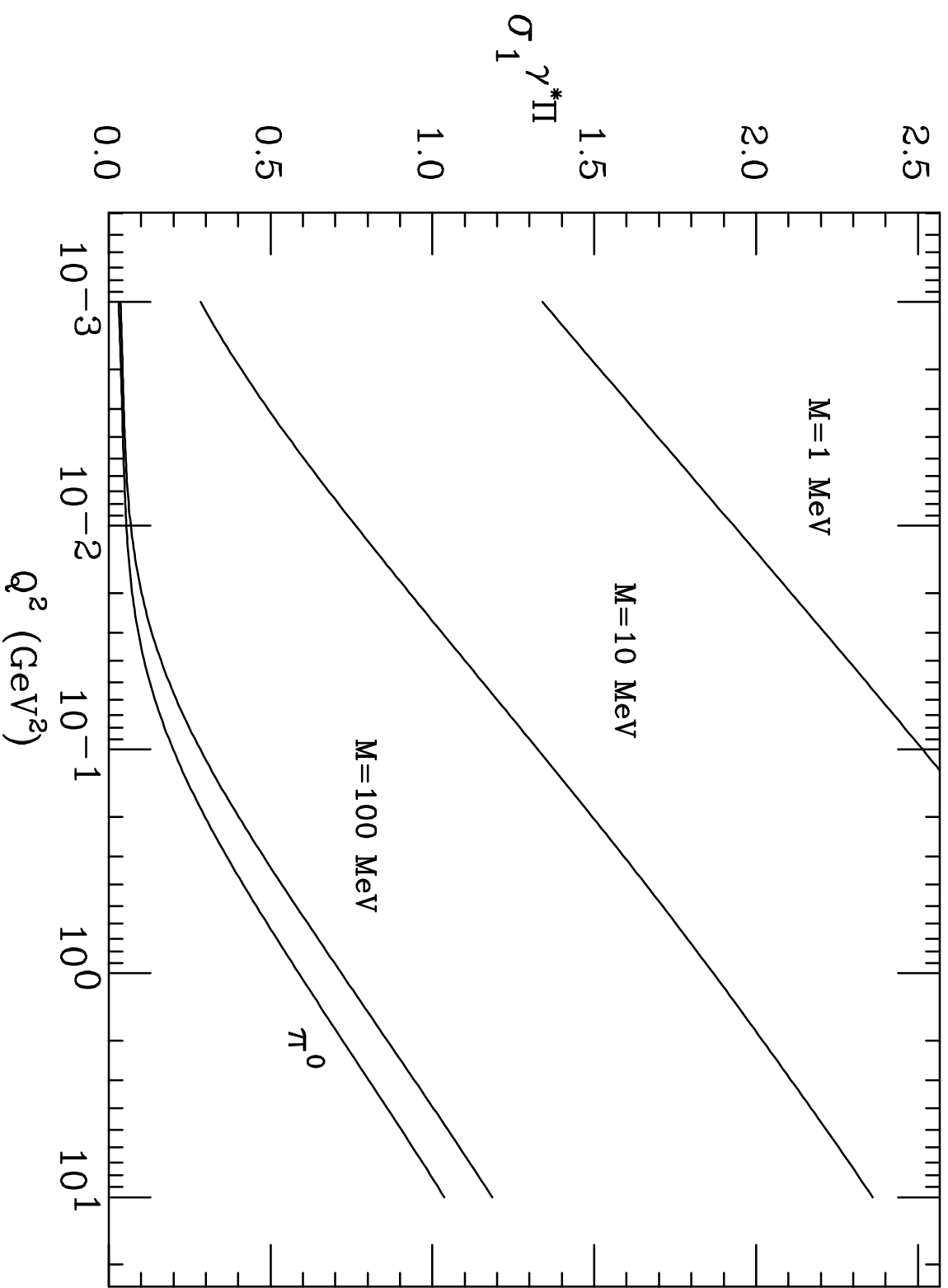


Fig. 10a

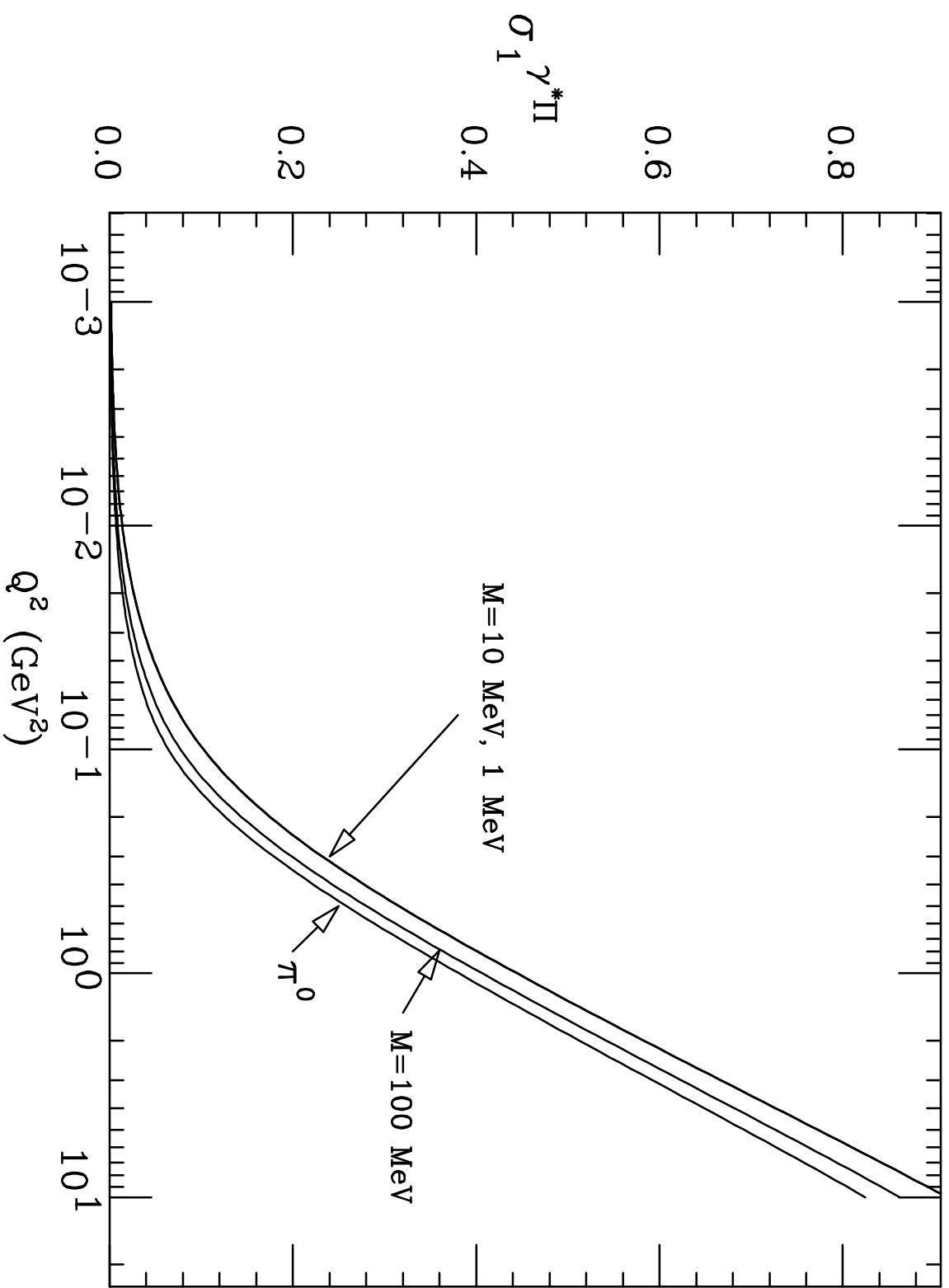


Fig. 10b

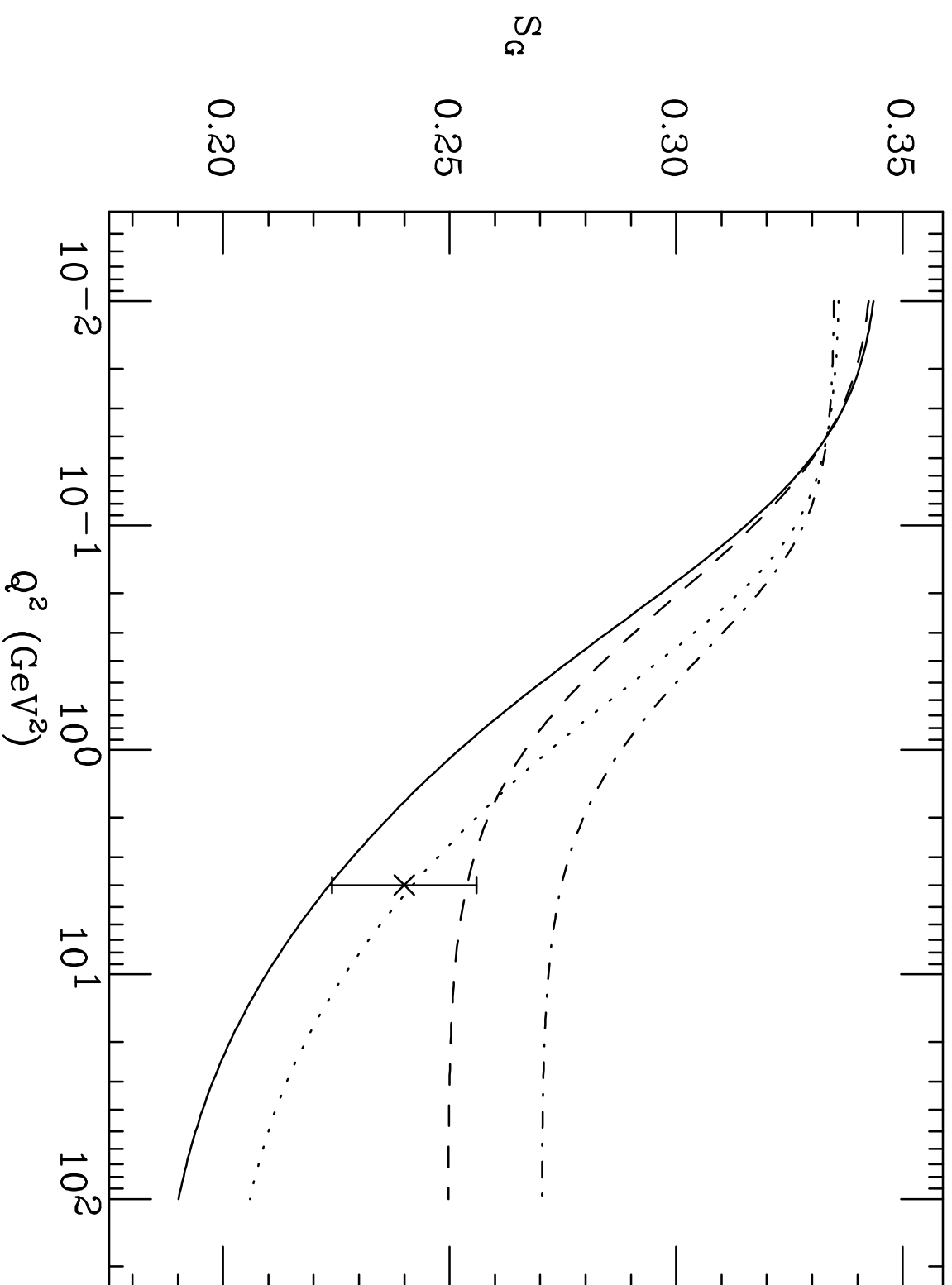


Fig. 11